Embedded Non-destructive Evaluation for Structural Health Monitoring, Damage Detection, and Failure Prevention

Victor Giurgiutiu and Adrian Cuc

ABSTRACT—In this paper we review the state of the art in an emerging new technology: embedded ultrasonic non-destructive evaluation (NDE). Embedded ultrasonic NDE permits active structural health monitoring, i.e. the on-demand interrogation of the structure to determine its current state of structural health. The enabling element of embedded ultrasonic NDE is the piezoelectric wafer active sensor (PWAS). We begin by reviewing the guided wave theory in plate, tube, and shell structures, with special attention to Lamb waves. The mechanisms of Lamb wave excitation and detection with embeddable PWAS transducers is presented. It is shown analytically and verified experimentally that Lamb wave mode tuning can be achieved by the judicious combination of PWAS dimensions, frequency value, and Lamb mode characteristics. Subsequently, we address in turn the use of pitch-catch, pulse-echo, and phased array ultrasonic methods for Lamb-wave damage detection. In each case, the conventional ultrasonic NDE results are contrasted with embedded NDE results. Detection of cracks, disbonds, delaminations, and diffuse damage in metallic and composite structures are exemplified. Other techniques, such as the time reversal method and the migration technique, are also presented. The paper ends with conclusions and suggestions for further work.

KEYWORDS: structural health monitoring, ultrasonic, Lamb waves, piezoelectric wafer active sensors, pitch-catch, pulse-echo, phased array, electromechanical impedance, damage detection, time reversal, migration technique, crack propagation, adhesives, adhesive joints, disbonds, diagnosis, prognosis, mixed-mode fracture, non-destructive evaluation, non-destructive inspection

1. Introduction

Structural health monitoring (SHM) is an emerging research area with multiple applications. SHM assesses the state of structural health and, through appropriate data processing and interpretation, predicts the remaining life of the structure. Many aerospace and civil infrastructure systems are at or beyond their design life; however, it is envisioned that they will remain in service for an extended period. SHM is one of the enabling technologies that will make this possible. Another potential SHM application is in new systems. By embedding SHM sensors and sensory systems into a new structure, the design paradigm can be changed and considerable savings in weight, size, and cost can be achieved. Not surprisingly, the SHM of aerospace structures has recently received increased attention (Associated Press, 2003; Butterworth-Hayes, 2003; Talbot, 2003; Staszewski et al., 2004)

1.1. Conventional Non-destructive Evaluation

There is a large number of non-destructive evaluation (NDE), non-destructive testing (NDT), and non-destructive inspection (NDI) techniques for identifying local damage and detect incipient failure in critical structures. Among them, ultrasonic inspection is well established and has been used in the engineering community for several decades (Krautkramer and Krautkramer, 1990).

In an infinite solid medium, elastic waves can propagate in two basic modes: pressure (P) waves and shear (S) waves. However, if the medium is bounded, wave reflections occur at the boundary and more complicated wave patterns emerge. Of particular interest are the guided waves, which remain contained in a wave guide and can travel at large distances. Lamb waves are guided waves traveling along thin plates, while Rayleigh waves are guided waves constraint to the surface. Guided waves can also exist in solid and hollow cylinders, as well as in shell structures. Love waves are guided waves traveling in layered materials, while Stoneley waves are guided waves constrained to the material interface. The early study of guided waves is credited to Rayleigh (1887), Lamb (1917), Love (1926, 1944), and Stoneley (1924). A comprehensive analysis of Lamb waves has been given by Viktorov (1967), Achenbach (1973), Graff (1975), Rose (1999), Royer and Dieulesaint (2000), and others.

Ultrasonic NDE methods rely on elastic wave propagation and reflection within the material. They try to identify the wave field disturbances due to local damage and flaws. Ultrasonic testing involves one or more of the following measurements: time of flight (TOF; wave transit or delay), path length, frequency, phase angle, amplitude, acoustic impedance, and angle of wave deflection (reflection and refraction). Conventional ultrasonic methods include the pulse-echo, the pitch-catch (or pulse-transmission), and the pulse-resonance techniques (Blitz and Simpson, 1996). A piezoelectric ultrasonic probe placed on the structural sur-

Victor Giurgiutiu (victorg@sc.edu) and Adrian Cuc,
University of South Carolina, Department of Mechanical Engineering, Columbia, SC 29208, USA.

The Shock and Vibration Digest, Vol. 37, No. 2, March 2005 83–105

DOI: 10.1177/0583102405052561

face induces ultrasonic waves in the material. Good contact between the transducer and the structure is obtained by using special coupling gels. Depending on the incidence of the transducer with respect to the structural surface, the waves created in the structures may be P, S, or a combination of the two. P-waves are best suited for through-the-thickness detection. They are very effective in detecting anomalies along the sound path. In the pulse-echo method, defects are detected in the form of additional echoes. In the pitch-catch method, wave dispersion and attenuation due to diffused damage in the material are used as flaw indicators.

For thickness-wise inspection, the sound path traverses only a small portion of the material volume; hence, the transducer is mechanically moved along the surface to scan and interrogate the entire material volume. Ultrasonic inspection of thin wall structures (e.g. aircraft shells, storage tanks, large pipes, etc.) is a time-consuming operation that requires meticulous through-the-thickness C-scans over large areas. If done improperly, it can miss essential flaws. In addition, ultrasonic waves cannot be induced at right angles to the structural surface. Localized surface flaws, and cracks with their plane perpendicular to the structural surface cannot be readily detected with through-the-thickness P-wave methods. However, guided waves have shown encouraging results in detecting these types of flaws. For the inspection of thin-wall structures, such as sheet-metal constructions, airframes, large containers, pipes, or tubes, an alternate inspection method utilizing guided Lamb waves may be more appropriate. Advanced ultrasonic techniques rely on the generation, propagation, and detection of Rayleigh, Lamb, and Love waves. These waves can be generated using conventional ultrasonic transducers and wedge couplers, provided the angle of the coupler is sufficiently large to trigger mode conversion. Alternatively, Lamb waves can be generated by comb transducers. Guided waves are being used to detect cracks, inclusions, and disbonds in metallic and composite structures. Lamb waves are appropriate for thin plate and shell structures, while Rayleigh waves are more useful for the detection of surface defects.

Worlton (1957, 1961) was among the first to recognize the advantages that Lamb and Rayleigh waves offer over P-waves for NDE applications. Viktorov (1967) studied the use of Rayleigh and Lamb waves for ultrasonic testing. Rose (1995) and Krautkramer (1998) reviewed the applications of portable guided wave ultrasonic devices for inspecting steam generator tubing, aging aircraft structures and some powder injected molded parts in manufacturing settings. Good sensitivity and range of detection were demonstrated. Recently, Rose (2001) has reiterated the inspection potential of ultrasonic guided waves for thin-wall structures. Guided Lamb waves offer an improved inspection potential due to:

- variable mode structure and distributions;
- multimode character;
- sensitivity to different types of flaws;
- propagation over long distances;
- guiding character, which enables them to follow curvature and reach hidden and/or buried parts.

The potential use of guided waves for monitoring metallic aircraft structures was investigated by Alleyne and Cawley (1992) and Dalton et al. (2001). Several issues were addressed: the selection of the Lamb wave modes, the effect of skin tapering, the effect of sealants and paints, the propagation across double skin systems, and the propagation across aircraft joints. The results have shown that guided waves offer good potential for localized structural monitoring. Long-range propagation through tapered skin presents little problem as long as dispersion is avoided. However, sealant layers can create severe damping problems. The effect of structural fasteners was not studied.

1.2. Structural Health Monitoring and Embedded Ultrasonic Non-destructive Evaluation

SHM sets out to determine the health of a structure by reading a network of sensors that are embedded (permanently attached) into the structure and monitored over time. SHM can be either passive or active. Passive SHM infers the state of the structure using passive sensors that are monitored over time and fed into a structural model. Examples of passive SHM are the monitoring of loads, stress, environmental conditions, acoustic emission from cracks, etc. Passive SHM only "listens" to the structure but does not interact with it. Kudva et al. (1993) and Van Way et al. (1995) presented passive SHM systems utilizing an assortment of sensors such as acoustic emission transducers, resistance strain gages, fiber optic strain gages, filament crack gages, and corrosive environment sensors. Boller et al. (1999) showed that the reliability of SHM systems increases when the sensors do not just "listen" but act as both actuators and sensors. Active SHM uses active sensors that interrogate the structure to detect the presence of damage, and to estimate its extent and intensity. One active SHM method employs piezoelectric wafer active sensors (PWAS), which send and receive ultrasonic Lamb waves and determine the presence of cracks, delaminations, disbonds, and corrosion. Two approaches are being considered: (a) traveling waves; (b) standing waves. Active sensors interact with the structure in much the same way that conventional NDE transducers do. For this reason, active SHM can be also viewed as embedded non-destructive evaluation (e-NDE), i.e. an NDE method that utilizes embedded transducers that are permanently attached to the structure and can be interrogated on demand. e-NDE is an emerging technology that will allow the transition of the conventional ultrasonic NDE methods to embedded applications in active SHM systems. Viewing active SHM from the e-NDE point of view allows us to draw on the experience already developed in the NDE field and to transition it into SHM applications.

This paper sets forth to introduce the reader to the general principles of e-NDE and to present some of the salient achievements in its application to active SHM. The paper starts with a brief review of guided wave theory in plate, tube, and shell structures. Then, it introduces the PWAS, which are the essential elements of e-NDE systems. Subsequently, the paper shows how the main NDE methods (pitch-catch and pulse-echo) are being used in e-NDE applications. Furthermore, in the paper we present the concept of embedded phased arrays, and demonstrate them with the embedded ultrasonics structural radar (EUSR). Other techniques such as the time reversal method and the migration technique are also presented. At the end, conclusions and suggestions for further work are presented.

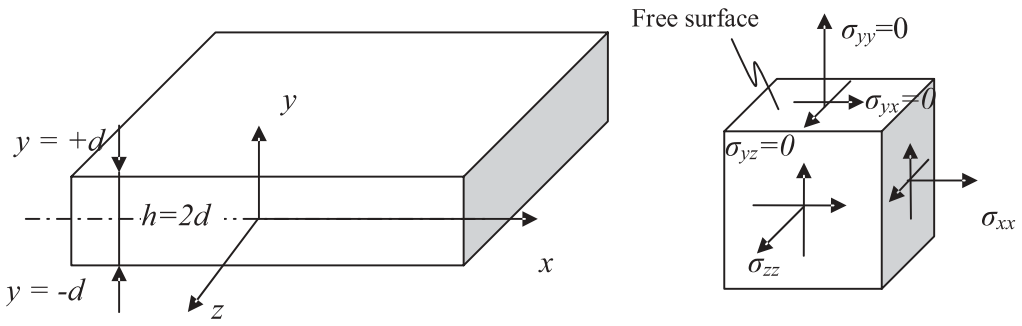

Figure 1. (a) A plate with thickness 2*d*, extending infinitely in *x* and *z* directions. (b) A free body diagram of an infinitesimal area extracted from the plate.

2. Guided Waves in Thin-wall Structures

Guided waves have the important property that they remain confined inside the walls of a thin-wall structure, and hence can travel over large distances. In addition, guided waves can also travel inside curved walls. These properties make them well suited for the ultrasonic inspection of aircraft, missiles, pressure vessel, oil tanks, pipelines, etc.

In flat plates, ultrasonic guided waves travel as Lamb waves and as shear horizontal (SH) waves. Lamb waves are vertically polarized, while SH waves are horizontally polarized. Both Lamb waves and SH waves can be symmetric or antisymmetric with respect to the plate mid-plane. A brief outline of the main equations is presented next, following Graff (1975). Consider a plate with stress-free upper and lower surfaces situated at $y = \pm d$ (Figure 1). The equation of motion for an isotropic elastic medium is given by

$$\mu\nabla^2\mathbf{u} + (\lambda+\mu)\nabla\nabla\bullet\mathbf{u} = \rho\frac{\partial^2\mathbf{u}}{\partial t^2} \tag{1}$$

where λ and μ are the Lamé constants, ρ is the mass density, and $\mathbf{u}$ is the displacement vector. Assume that the displacement vector is given by

$$\mathbf{u} = \nabla\Phi + \nabla\times\mathbf{H} \tag{2}$$

where Φ and $\mathbf{H}$ are the potential functions given by

$$\begin{aligned}\Phi &= f(y)e^{i(\xi x-\omega t)},\\ \mathbf{H} &= (h_x(y)\mathbf{i} + h_y(y)\mathbf{j} + h_z(y)\mathbf{k})e^{i(\xi x-\omega t)}.\end{aligned} \tag{3}$$

Straight crested waves of circular frequency ω and wavenumber ξ propagating with wave speed $c = \omega/\xi$ were assumed. The governing equations are

$$\nabla^2\Phi = \frac{1}{c_p^2}\frac{\partial^2\Phi}{\partial t^2}, \quad \nabla^2\mathbf{H} = \frac{1}{c_s^2}\frac{\partial^2\mathbf{H}}{\partial t^2}, \quad \text{and} \quad \nabla\bullet\mathbf{H} = 0. \tag{4}$$

Plane strain (*z*-invariant) conditions are assumed. Hence, equation (4) yields

$$\begin{aligned}f'' - \xi^2 f &= -\omega^2 f/c_p^2\\ h_x'' - \xi^2 h_x &= -\omega^2 h_x/c_s^2\\ h_y'' - \xi^2 h_y &= -\omega^2 h_y/c_s^2\\ h_z'' - \xi^2 h_z &= -\omega^2 h_z/c_s^2\end{aligned} \tag{5}$$

where $c_p^2 = (\lambda+2\mu)/\rho$ and $c_s^2 = \mu/\rho$ are the pressure (longitudinal) and shear (transverse) wave speeds. Solution of equation (5) is in the form

$$\begin{aligned}\Phi &= (A\cos\alpha y + B\sin\alpha y)e^{i(\xi x-\omega t)}\\ H_x &= (C\cos\beta y + D\sin\beta y)e^{i(\xi x-\omega t)}\\ H_y &= (E\cos\beta y + F\sin\beta y)e^{i(\xi x-\omega t)}\\ H_z &= (G\cos\beta y + H\sin\beta y)e^{i(\xi x-\omega t)}\end{aligned} \tag{6}$$

where $\alpha^2 = (\omega^2/c_p^2) - \xi^2$, and $\beta^2 = (\omega^2/c_s^2) - \xi^2$. The constants $A - H$ are determined from the stress-free boundary conditions at the plate upper and lower surfaces, which yield

$$\begin{bmatrix}
-c_3\sin\alpha d & c_4\sin\beta d & 0 & 0 & 0 & 0 & 0 & 0\\
c_1\cos\alpha d & c_2\cos\beta d & 0 & 0 & 0 & 0 & 0 & 0\\
0 & 0 & c_1\sin\alpha d & -c_2\sin\beta d & 0 & 0 & 0 & 0\\
0 & 0 & c_3\cos\alpha d & c_4\cos\beta d & 0 & 0 & 0 & 0\\
0 & 0 & 0 & 0 & -c_5\sin\beta d & \beta^2\sin\beta d & 0 & 0\\
0 & 0 & 0 & 0 & -\beta\sin\beta d & i\xi\sin\beta d & 0 & 0\\
0 & 0 & 0 & 0 & 0 & 0 & \beta^2\cos\beta d & c_5\cos\beta d\\
0 & 0 & 0 & 0 & 0 & 0 & i\xi\cos\beta d & \beta\cos\beta d
\end{bmatrix}
\begin{bmatrix}A\\H\\B\\G\\E\\D\\C\\F\end{bmatrix} = 0 \tag{7}$$

with $c_1 = (\lambda+2\mu)\alpha^2 + \lambda\xi^2$, $c_2 = 2i\mu\xi\beta$, $c_3 = 2i\xi\alpha$, $c_4 = \xi^2 - \beta^2$, $c_5 = i\xi\beta$. Non-trivial solutions of the homogeneous equation (7) are obtained when the determinant of the coefficients matrix is zero, which yields the characteristic equation. Examination of equation (7) reveals that the determinant can be broken up into the product of four smaller determinants, corresponding to the coefficient pairs (*A, H*), (*B, G*), (*E, D*), and (*C, F*). The first two pairs correspond to the symmetric and antisymmetric Lamb waves, while the last two pairs correspond to symmetric and antisymmetric SH

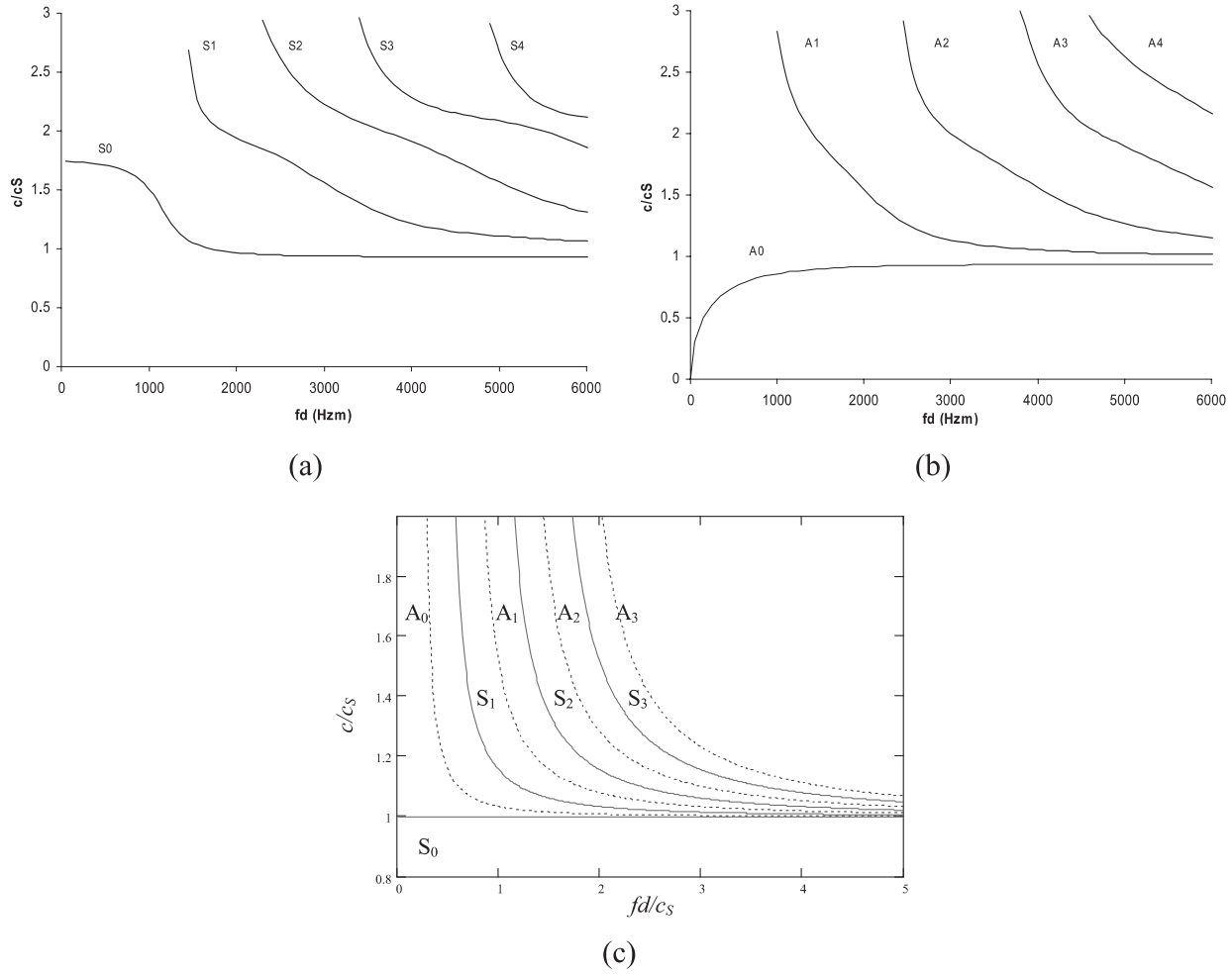

Figure 2. Wave speed dispersion curves in plates: (a) symmetric Lamb waves, S_n; (b) antisymmetric Lamb waves, A_n; (c) SH waves: solid lines are for symmetric SH modes (S_n), dotted lines are for antisymmetric SH modes (A_n) (c_S is the shear wave speed, and d is the half-thickness of the plate).

waves. The characteristic equations for the symmetric and antisymmetric Lamb waves are also know as the Rayleigh–Lamb equations**.** These implicit transcendental equations are solved numerically to determine the permissible guided-wave solutions. For each solution of the characteristic equation, one determines a specific value of the wavenumber, ξ, and hence the wave speed, c.

The variation of wave speed with frequency is shown in Figure 2(a) and (b) for Lamb waves, and in Figure 2(c) for SH waves. At lower frequency-thickness products, only two Lamb wave types exist: S_0, which is a symmetrical Lamb wave resembling the longitudinal waves, and A_0, which is an antisymmetric Lamb wave resembling the flexural waves. At higher frequency-thickness values, a number of Lamb waves are present, S_n and A_n, where $n = 0, 1, 2,\ldots$. At very high frequencies, the S_0 and A_0 Lamb waves coalesce into the Rayleigh waves, which are confined to the plate upper and lower surfaces. The Lamb waves are highly dispersive (wave speed varies with frequency); however, S_0 waves at low frequency-thickness values show very little dispersion. The SH waves are also dispersive, with the exception of the first mode, SH_0, which does not show any dispersion at all.

For circular crested waves, a similar analysis can be conducted in polar coordinates. Goodman (1952) investigated circular crested Lamb waves, and developed solutions in terms of Bessel functions J_0 and J_1. He showed that the Rayleigh–Lamb frequency equations developed for straight crested Lamb waves also apply to circular crested Lamb waves. For large radii, the circular crested Lamb waves attain a uniform wavelength that correlates with that of straight crested Lamb waves. However, the amplitude of a circular crested Lamb wave decreases with the square root of the radius, which confirms simple energy conservation considerations.

In shell structures, guided waves can propagate in a variety of modes. The study of guided wave propagation in cylindrical shells can be considered as a limiting case of the study of guided wave propagation in hollow cylinders. As the wall thickness of a hollow cylinder decreases with respect to its radius, the hollow cylinder approaches the case of a thin-wall cylindrical shell. Comprehensive analytical

and numerical results on wave propagation in hollow circular cylinders were presented by Gazis (1959). The nonlinear algebraic equations and the corresponding numerical solutions of the wave speed dispersion curves were obtained. These results found important applications in the ultrasonic NDE of tubing and pipes. Silk and Bainton (1979) found equivalences between the ultrasonic waves in hollow cylinders and the Lamb waves in flat plates, and used them to detect cracks in heat exchanger tubing. Rose et al. (1994) used guided waves to find cracks in nuclear steam generator tubing. Alleyne et al. (2001) used guided waves to detect cracks and corrosion in chemical plant pipework. A brief review of the mathematical modeling and the main results for guided waves in cylindrical shells are given next (Gazis, 1959; Zemenek, 1972; Silk and Bainton, 1979; Rose et al., 1994). Consider a circular cylinder of inner and outer radii a and b, and thickness h. In cylindrical coordinates (r, θ, z), the potential functions are expressed as

$$\begin{aligned} \phi &= f(r)\cos n\theta \cos(\omega t + \xi z) \\ H_r &= h_r(r)\sin n\theta \sin(\omega t + \xi z) \\ H_\theta &= h_\theta(r)\cos n\theta \sin(\omega t + \xi z) \\ H_z &= h_z(r)\sin n\theta \cos(\omega t + \xi z) \end{aligned} \tag{8}$$

where wave motion along the z-axis with wavenumber ξ is assumed. Substitution of equation (8) into equation (4) yields

$$\begin{aligned} (\nabla^2 + \omega^2/c_p^2)\phi &= 0 \\ (\nabla^2 + \omega^2/c_s^2)H_z &= 0 \\ (\nabla^2 - 1/r^2 + \omega^2/c_s^2)H_r - (2/r^2)(\partial H_\theta/\partial\theta) &= 0 \\ (\nabla^2 - 1/r^2 + \omega^2/c_s^2)H_\theta + (2/r^2)(\partial H_r/\partial\theta) &= 0. \end{aligned} \tag{9}$$

The general solution is expressed in terms of Bessel functions J and Y or the modified Bessel functions I and K of arguments $\alpha_1 r = |\alpha r|$ and $\beta_1 r = |\beta r|$. The general solution is of the form

$$\begin{aligned} f &= A \cdot Z_n(\alpha_1 r) + B \cdot W_n(\alpha_1 r) \\ h_3 &= A_3 \cdot Z_n(\beta_1 r) + B_3 \cdot W_n(\beta_1 r) \\ h_1 &= \frac{1}{2}(h_r - h_\theta) = A_1 \cdot Z_{n+1}(\beta_1 r) + B_1 \cdot W_{n+1}(\beta_1 r) \\ h_2 &= \frac{1}{2}(h_r + h_\theta) = A_2 \cdot Z_{n-1}(\beta_1 r) + B_2 \cdot W_{n-1}(\beta_1 r) \end{aligned} \tag{10}$$

where, for brevity, Z denotes a J or I Bessel function, and W denotes a Y or a K Bessel function, as appropriate. Thus, the potentials are expressed in terms of the unknowns A, B, A_1, B_1, A_2, B_2, A_3, and B_3. Two of these unknowns are eliminated using the gage invariance property of the equivolume potentials. Imposing the stress-free boundary conditions at the inner and outer radii, a and b, yields a linear system of six homogeneous equations in six unknowns. For non-trivial solution, the system determinant must vanish, i.e.

$$|c_{ij}| = 0\,,\ i,j = 1,\ldots,6. \tag{11}$$

The coefficients c_{ij} in equation (11) have complicated algebraic expressions that are omitted for brevity. The result is a characteristic equation in the form:

$$\Omega_n(a, b, \lambda, \mu, fd, c) = 0. \tag{12}$$

This implicit transcendental equation is solved numerically for the permissible guided wave solutions. As shown by Gazis (1959), three basic guided wave families exist:

- longitudinal axially symmetric modes, L(0, m), m = 1, 2, 3, …;
- torsional axially symmetric modes, T(0, m) , m = 1, 2, 3, …;
- flexural non-axially symmetric modes, F(n, m), n = 1, 2, 3, … m = 1, 2, 3, ….

Within each family, an infinite number of modes exist such that their phase velocities, c, for a given frequency-thickness product, fd, represent permissible solutions of the implicit transcendental equation (12). The index m represents the number of the mode shapes across the wall of the tube. The index n determines the manner in which the fields generated by the guided wave modes vary with angular coordinate θ in the cross-section of the cylinder. For the F modes of index n, each component can be considered to vary as either $\sin(n\theta)$ or $\cos(n\theta)$. It is also observed that the index n = 1 represents the mode shape of flexing the tube as a whole.

The longitudinal and torsional modes are also referred to as the axial symmetric or n = 0 modes. These axial symmetric modes are preferred for defect detection in long pipes since the pipe circumference is uniformly insonified. The longitudinal modes are easier to generate with conventional ultrasonic transducers. They are good for the location of circumferential cracks. However, for the location of axial cracks and corrosion, the torsional modes, although more difficult to generate with conventional ultrasonic transducers, are recommended.

An examination of the differential equation dependence on the ratios h/r and h/λ indicates that, for shallow shells (h/r and $h/\lambda << 1$), the longitudinal modes approach the Lamb wave modes, whereas the torsional modes approach the SH modes. In fact, it can be shown that the L(0,1) mode corresponds to the A_0 Lamb mode, while the L(0,2) mode corresponds to the S_0 Lamb mode, etc. The flexural modes remain a mode-type specific to tube waves and without equivalence in flat plate waves.

3. Piezoelectric Wafer Active Sensors

Guided waves can be excited and detected with a variety of methods. In conventional ultrasonics, guided waves are generated by impinging the structural surface obliquely with an ultrasonic beam from a relatively large ultrasonic transducer affixed to a wedge. Snell's law ensures mode conversion at the interface; hence, a combination of pressure and shear waves are simultaneously generated into the structure. If the structure is thin-walled, guided waves are being created. Another method of creating guided waves in a structure is by using a comb transducer. The comb spacing is such that it tunes with the guided wave half-wavelength.

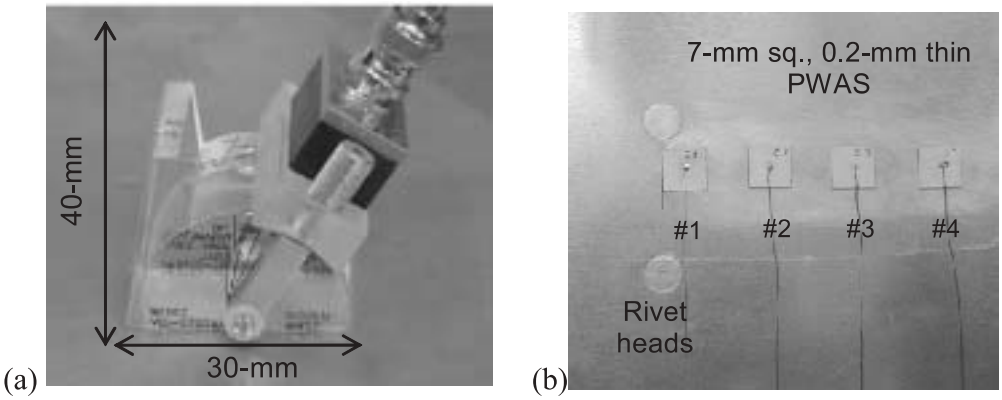

Figure 3. (a) Conventional Lamb wave ultrasonic transducer (~25 g, ~$400, 40 mm tall). (b) PWAS (0.08 g, $15, 0.2 mm thin).

However, conventional Lamb wave probes (wedge and comb transducers) are relatively too heavy and expensive to be considered for widespread deployment on an aircraft structure as part of an active SHM system. A typical wedge transducer weighs 25 g, costs ~$400, and is 40 mm tall (Figure 3(a)). Conventional ultrasonic transducers are inappropriate for active SHM applications due to their cost, weight, and size. Conventional ultrasonic transducers could not be embedded in large numbers into a structure without incurring important cost and weight penalties.

An automated SHM system embedded into the aircraft structure is not possible using conventional ultrasonic transducers. For such a system, the sensors must be as much as possible part of the structure on which they are attached. Hence, active sensors that are different from the conventional ultrasonic transducers are required. New types of Lamb wave transducers must be developed; they must be small, lightweight, unobtrusive, and low cost. They should be embedded in the airframe with minimum weight penalty and at affordable costs. In recent years, piezoelectric wafers permanently attached to the structure have been extensively used for the generation and detection of guided waves. These simple devices are inexpensive, lightweight, and unobtrusive (Figure 3(b)). They seem well suited for SHM applications. They can act as both transmitters and receivers of ultrasonic waves. For lack of a better term, Giurgiutiu et al. (2000) called these embedded transducers PWAS. Typical PWAS weigh around 68 mg, are 0.2 mm thick, and cost ~$15 each. Giurgiutiu and Zagrai (2000) characterized the PWAS for SHM and developed quality assurance techniques. Lamb wave NDE techniques are being transitioned to embedded applications using PWAS technology.

3.1. Piezoelectric Wafer Active Sensors Principles

PWAS are small and lightweight. They are also relatively low cost. PWAS can be bonded to the structure (Figure 3(b)), or inserted into the layers of a composite structure. When permanently attached/embedded into the structure, PWAS provide the bidirectional energy transduction from the electronics into the structure, and from the structure back into the electronics. PWAS achieve direct transduction of electric energy into elastic energy, and vice versa. PWAS were initially used by Crawley and de Luis (1987), Crawley and Anderson (1990) and others for structural vibration control. The use of PWAS in active SHM has been explored experimentally by Chang (1995, 1998), Keilers and Chang (1995), Lakshmanan and Pines (1997), Moulin et al. (1997), Wang and Chang (1999), Dupont et al. (2000), Monier et al. (2000), Lin and Yuan (2001a,b,c), Diamanti et al. (2002), Kessler (2002), Ihn and Chang (2002), Koh et al. (2003), and others. Pitch-catch, pulse-echo, and even phased arrays have been experimentally demonstrated (Giurgiutiu et al., 2000, 2003; Giurgiutiu and Bao, 2002). These successful experiments have positioned PWAS as an enabling technology for active SHM implementation.

PWAS operate on the piezoelectric principle that couples the electrical and mechanical variables in the material (mechanical strain, S_{ij}, mechanical stress, T_{kl}, electrical field, E_k, and electrical displacement D_j) in the form

$$\begin{aligned} S_{ij} &= s^E_{ijkl} T_{kl} + d_{kij} E_k \\ D_j &= d_{jkl} T_{kl} + \varepsilon^T_{jk} E_k \end{aligned} \tag{13}$$

where s^E_{ijkl} is the mechanical compliance of the material measured at zero electric field ($E = 0$), ε^T_{jk} is the dielectric permittivity measured at zero mechanical stress ($T = 0$), and d_{kij} represents the piezoelectric coupling effect. The direct piezoelectric effect converts the stress applied to the sensor into electric charge. Similarly, the converse piezoelectric effect produces strain when a voltage is applied to the sensor. For e-NDE applications, PWAS couple their in-plane motion, electrically excited through the piezoelectric effect, with the Lamb wave particle motion on the material surface (Figure 4). Lamb waves can be either quasi-axial (S_0, S_1, S_2, …), or quasi-flexural (A_0, A_1, A_2, …). PWAS transducers can act as both exciters and detectors of the elastic Lamb waves traveling in the material. PWAS can be used as both active and passive probes and thus can address four SHM needs:

(1) active sensing of far-field damage using pulse-echo, pitch-catch, and phased-array methods;
(2) active sensing of near-field damage using the high-frequency impedance method;

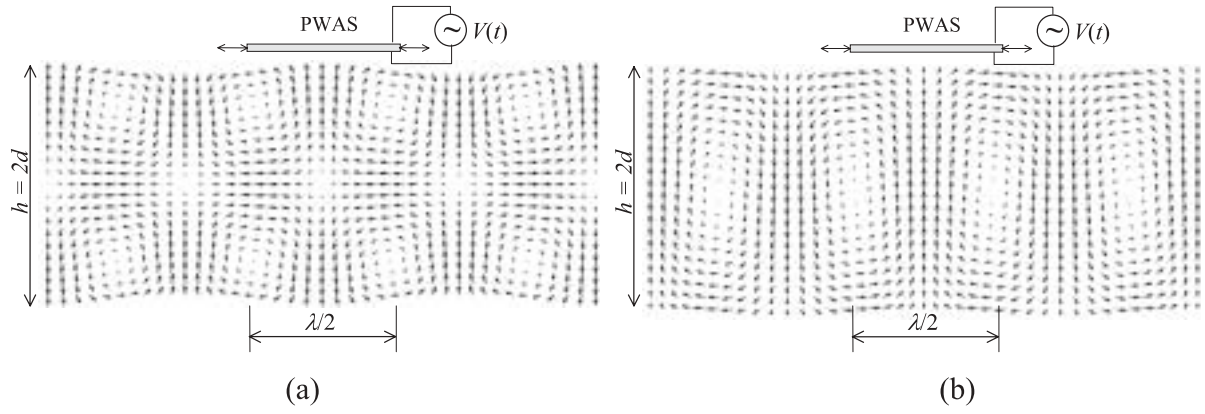

Figure 4. Simulation of Lamb wave motion in a 1 mm thick aluminum plate: (a) symmetric mode S_0, $f = 1.56$ MHz; (b) antisymmetric mode A_0, $f = 0.788$ MHz.

(3) passive sensing of crack initiation and growth through acoustic emission;
(4) passive sensing of damage-generating events through low-velocity impact detection.

This indicates that the PWAS transducers are strong candidates for active SHM applications.

At first sight, PWAS may seem very similar to the conventional ultrasonic transducers since both use the piezoelectric effect. However, fundamental differences exist between the conventional ultrasonic transducers and the PWAS.

(1) Conventional ultrasonic transducers are weakly coupled with the structure through gel, water, or air. In contrast, PWAS are strongly coupled with the structure through an adhesive bond.
(2) Conventional ultrasonic transducers are resonant narrow-band devices. In contrast, PWAS are non-resonant broad-band devices that can be tuned selectively into certain Lamb modes.
(3) Conventional ultrasonic transducers excite and sense the Lamb waves in the structure indirectly through acoustic waves impinging on the structural surface and the mode conversion. In contrast, PWAS excite and sense the Lamb waves in the structure directly through in-plane strain coupling.

PWAS-based embedded ultrasonics bears substantially on the experience accrued with conventional ultrasonic transducers. However, major differences exist between conventional ultrasonics and embedded ultrasonics. Drawbacks of the conventional ultrasonics are the bulkiness of transducers and the need for a normal (perpendicular) interface between the transducer and the test structure. The former limits the access of ultrasonic transducers to restricted spaces; the latter influences the type of waves that can be easily generated in the structure. In contrast, embedded ultrasonics uses PWAS that are permanently bonded to the structural surface and are small, thin, unobtrusive, and non-invasive. They can be placed in very restrictive spaces, such as in built-up aerospace structures. The surface-bonded PWAS can easily produce guided waves traveling parallel to the surface and can detect damage that would escape a conventional ultrasonic method. In their simplest form, PWAS are just thin piezoelectric ceramic wafers. However, ceramics are rather brittle, vulnerable to crack damage, and non-conformable to curved surfaces. To address these aspects, new devices are being developed, such as the macrofiber composite (e.g. Williams et al., 2002) and active fiber composites (e.g., Janos and Hagood, 1998).

3.2. Selective Lamb Wave Mode Tuning with PWAS

An important characteristic of PWAS, which distinguishes them from conventional ultrasonic transducers, is their capability of tuning into various guided wave modes. Moulin et al. (1997) were among the first to realize the generation of Lamb waves with embedded piezoelectric disks. Using finite element modeling and experimental results, they showed the excitation of S_0, S_1, A_0, A_1, and A_2 Lamb waves at up to 2.5 MHz frequencies. Lin and Yuan (2001a) studied the use of piezoceramic disks for the generation and detection of circular-crested flexural waves in a composite plate using the Mindlin theory. The solution was derived in terms of Henkel functions. Propagation of smoothed tone-bursts was studied. The theoretical predictions compared favorably with experimental measurements. Liu et al. (2003) investigated the input–output characteristics of piezoelectric SHM systems for composite plates. Lee and Staszewski (2003) used finite differences and the local interaction simulation approach (LISA) to model the generation of Lamb waves with surface-mounted piezoceramic wafers for the detection of structural damage. Numerical simulation compared favorably with experiments. Qing et al. (2003) reported experimental results indicating that PWAS effectiveness in exciting A_0 and S_0 Lamb modes varies significantly with the PWAS location across the laminate thickness.

Although a complete modeling of this interaction is not yet available, some simplified models exist that clarify the underlying principles of Lamb wave tuning with PWAS transducers. Giurgiutiu (2003) developed a plane-strain analysis of the PWAS–structure interaction using the space-

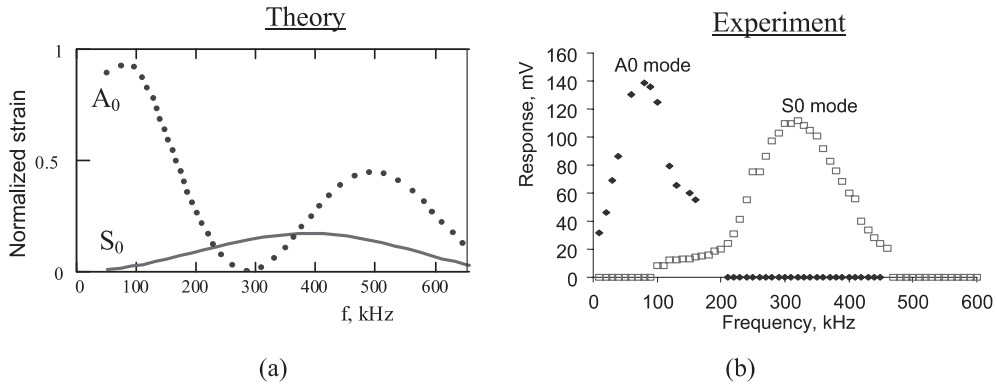

Figure 5. (a) Predicted Lamb wave strain amplitude in a 1.6 mm aluminum plate under a 7 mm PWAS excitation. (b) Experimental verification of excitation sweet spot at 300 kHz (Giurgiutiu, 2003).

domain Fourier analysis. This model illustrates the principles of PWAS Lamb wave mode tuning, and opens the path for a more comprehensive analysis. The analysis starts with transformed equations

$$\frac{d^2\tilde{\phi}}{dy^2} + p^2\tilde{\phi} = 0, \quad \frac{d^2\tilde{\psi}}{dy^2} + q^2\tilde{\psi} = 0$$
$$p^2 = \frac{\omega^2}{c_L^2} - \xi^2, \quad q^2 = \frac{\omega^2}{c_T^2} - \xi^2 \tag{14}$$

where $\tilde{\phi}$ and $\tilde{\psi}$ are the transformed potential functions, $c_L^2 = (\lambda + 2\mu)/\rho$ and $c_T^2 = \mu/\rho$ are the longitudinal (pressure) and transverse (shear) wave speeds, λ and μ are Lamé constants, and ρ is the mass density. The excitation is assumed in the form of time-harmonic shear stress, $\tau_a(x)e^{-i\omega t}$, applied by the PWAS to the structural surface over the interval $-a < x < +a$. Assuming perfect bonding between PWAS and structure concentrates the shear transfer effects at the PWAS ends. Hence, the shear stress $\tau(x)$ and its Fourier transform $\tilde{\tau}(\xi)$ are given by

$$\tau(x) = a\tau_0[\delta(x-a) - \delta(x+a)],$$
$$\tilde{\tau}(\xi) = a\tau[-2i\sin\xi a] \tag{15}$$

where $\delta(x)$ is the Dirac function. Equations (14) and (15) accept the Fourier-domain solution

$$\tilde{\varepsilon}_x = -i\frac{\tilde{\tau}}{2\mu}\left(\frac{N_S}{D_S} + \frac{N_A}{D_A}\right), \quad \tilde{u}_x = -i\frac{\tilde{\tau}}{2\mu}\frac{1}{\xi}\left(\frac{N_S}{D_S} + \frac{N_A}{D_A}\right) \tag{16}$$

where $\tilde{\varepsilon}_x$ is the axial strain, $\tilde{u}_x$ is the axial displacement, and

$$N_s = \xi q(\xi^2 + q^2)\cos ph\cos qh,$$
$$D_S = (\xi^2 - q^2)^2\cos ph\sin qh + 4\xi^2 pq\sin ph\cos qh$$
$$N_A = \xi q(\xi^2 + q^2)\sin ph\sin qh, \tag{17}$$
$$D_A = (\xi^2 - q^2)^2\sin ph\cos qh + 4\xi^2 pq\cos ph\sin qh.$$

Applying the inverse Fourier transform in the space domain, and adding the time-domain harmonic behavior yield the forward wave solution:

$$\varepsilon_x(x,t) = \frac{1}{2\pi}\frac{-i}{2\pi}\int_{-\infty}^{\infty}\left(\frac{\tilde{\tau}N_S}{D_S} + \frac{\tilde{\tau}N_A}{D_A}\right)e^{i(\xi x - \omega t)}d\xi,$$
$$u_x(x,t) = \frac{1}{2\pi}\frac{-i}{2\pi}\int_{-\infty}^{\infty}\frac{1}{\xi}\left(\frac{\tilde{\tau}N_S}{D_S} + \frac{\tilde{\tau}N_A}{D_A}\right)e^{i(\xi x - \omega t)}d\xi. \tag{18}$$

The integral in equation (18) is singular at the roots of D_S and D_A. These roots correspond to the symmetric and antisymmetric Lamb wave modes having eigenvalues, $\xi_0^S, \xi_1^S, \xi_2^S, \ldots, \xi_0^A, \xi_1^A, \xi_2^A, \ldots$. The integral in equation is evaluated through the residue theorem, using a semicircular contour consisting in the upper half of the complex ξ plane. Hence,

$$\varepsilon_x(x,t) = -i\frac{a\tau_0}{\mu}\sum_{\xi^S}\sin\xi^S a\frac{N_S(\xi^S)}{D_S'(\xi^S)}e^{i(\xi^S x - \omega t)}d\xi$$
$$- i\frac{a\tau_0}{\mu}\sum_{\xi^A}\sin\xi^A a\frac{N_A(\xi^A)}{D_A'(\xi^A)}e^{i(\xi^A x - \omega t)}d\xi. \tag{19}$$

The summations in equation (19) cover all the symmetric (ξ^S) and antisymmetric (ξ^A) Lamb wave modes that exist for a given value of ω in a given plate (Giurgiutiu, 2003).

A plot of this solution in the 0–1000 kHz bandwidth is presented in Figure 5a. The $\sin\xi a$ contained in equation (19) displays maxima when the PWAS length $l_a = 2a$ equals an odd multiple of the half-wavelength, and minima when it equals an even multiple of the half-wavelength. Several such maxima and minima exist, each associated with a certain Lamb mode of its own wavelength. These minima and maxima allow us to achieve Lamb mode tuning. We can tune into a selected Lamb mode by choosing the appropriate frequency and PWAS geometry. Figure 5(a) illustrates the tuning of the S_0 mode at 300 kHz. This occurs because, at this frequency, the amplitude of the A_0 mode goes through zero while that of the S_0 is still strong. Thus, we have tuning of the S_0 mode, and rejection of the A_0 mode. Figure 5(b)

shows the experimental confirmation of this S_0 "sweet spot". Lamb wave mode tuning offers considerable advantages. It allows us to select Lamb wave modes that are most appropriate for the particular application being considered. The tuning of the S_0 mode is important for the detection of certain defects, such as cracks. The S_0 mode is less dispersive than the A_0 mode at low *fd* values and produces better wave packets. When the A_0 mode is rejected, the remaining S_0 mode gives loud and clear pulse-echo reflections from the through-the-thickness cracks (Giurgiutiu et al., 2003).

Extension of this approach to circular crested Lamb waves was studied by Raghavan and Cesnik (2004). The equations are set in polar coordinates around a piezoelectric disk attached to the plate surface. The appropriate space-domain integral transform is the Hankel transform

$$\begin{aligned} \tilde{f}_n(\xi) &= \int_0^\infty f(r) J_n(\xi r) r \, \mathrm{d}r, \\ f(r) &= \int_0^\infty \tilde{f}_n(\xi) J_n(\xi r) \xi \, \mathrm{d}\xi, \end{aligned} \tag{20}$$

where $J_n(\,)$ is the Bessel function of order n. The solution is derived in terms of Bessel and Hankel functions.

4. Pitch-catch Embedded Ultrasonics Non-destructive Evaluation for Crack and Delamination Detection

The pitch-catch method can be used to detect structural changes that take place between a transmitter transducer and a receiver transducer. The detection is performed through the examination of the guided wave amplitude, phase, dispersion, and TOF in comparison with a "pristine" situation. Guided wave modes that are strongly influenced by small changes in the material stiffness and thickness (such as the A_0 Lamb wave) are well suited for this method. Typical applications include: (a) corrosion detection in metallic structures; (b) diffused damage in composites; (c) disbond detection in adhesive joints; (d) delamination detection in layered composites, etc. Further advancements in this direction were achieved through acousto-ultrasonics (Duke, 1988). The pitch-catch method can also be used to detect the presence of cracks from the wave signal diffracted by the crack.

4.1. Disbonds and Delamination Detection with Conventional Ultrasonics

Ultrasonic testing of adhesively bonded joints using guided waves for both aerospace and automotive applications is gaining more and more attention. In the NDE of adhesively bonded joints, of particular interest are the Lamb waves. Lamb wave methods have considerable potential for the inspection of adherent assemblies for two reasons: they do not require direct access to the bond region, and they are much more amenable to rapid scanning than are pressure wave techniques. Lamb waves can be excited in one plate of a bonded assembly, propagated across the joint region, and received in the second plate of the assembly. Inspection of the joint then would be based on the differences between the signals received on one side of the assembly compared to those transmitted on the other side.

Lowe and Cawley (1994) studied the applicability of plate wave techniques for inspection of adhesive and diffusion bonded joints. They found that the Lamb wave techniques are sensitive to the material properties and the thickness of the adhesive layer. Rose et al. (1995) used the ultrasonic guided waves for NDE of adhesively bonded structures. They developed a double spring hopping probe (DHSP) to introduce and receive Lamb waves. This method was used to inspect a lap splice joint of a Boeing 737-222. Preliminary results showed the method's capability of disbond detection. The severe corrosion area was also pointed out using the DHSP handheld device. Chona et al. (2003) used laser-generated Lamb waves to detect disbonds and delaminations in layered materials using a pitch-catch approach. They showed that A_0 are sensitive to damage associated with disbonds and delaminations in a multilayer material. Lee et al. (2004) studied the problem of wave propagation in a diffusion bonded model using spectral elements (SEs) and a new local interaction simulation approach (LISA) for numerical modeling. The novelty of their work was the sensor/actuator configuration consisting of five different layers of materials with one piezoceramic element generating a thickness mode vibration. The five layers were: two piezoelectric elements used for actuating and sensing (Sonox P5), two copper layers, and in the middle a couplant layer. The experiments validated the numerical simulation, showing that the actuator/sensor configuration could operate either in S_0 or A_0 modes using excitation frequencies of 260.5 and 100 kHz, respectively. However, the coupling layer distorts the wave propagation, due to its low impedance at the interface and low wave speed within the couplant medium.

Repair patches are widely used in the aircraft industry for small repairs of the aircraft fuselage in order to extend the operational life of aging aircrafts. Lamb waves can be successfully used to detect disbonds of composite repair patches (Rose et al., 1996).

4.2. Embedded Pitch-catch Non-destructive Evaluation

The pitch-catch method detects damage from the changes in the Lamb waves traveling through a damaged region. The method uses the transducers in pairs: one as transmitter, the other as receiver. In the embedded pitch-catch method (Figure 6), the transducers are either permanently attached to the structure or inserted between the layers of composite layup. Early studies in embedded pitch-catch NDE leveraged on surface acoustic wave (SAW) technology (SAW devices have been extensively studied as delay lines in radar applications). Culshaw and co-workers (Pierce et al., 1997, 2000; Gachagan et al., 1999) have studied the use of piezoelectric transmitters and optical-fiber receivers for damage detection in composite plates using ultrasonic Lamb waves. Conventional ultrasonic transducers, interdigital piezoelectric transducers, and simple PWAS were used. It was remarked that the PWAS gave good results in spite of their constructive simplicity.

Interdigital polyvinylidene difluoride (PVDF; a piezoelectric polymer) transducers were developed for the generation and detection of Lamb waves in e-NDE applications (Monkhouse et al., 1996, 2000). These transducers were able

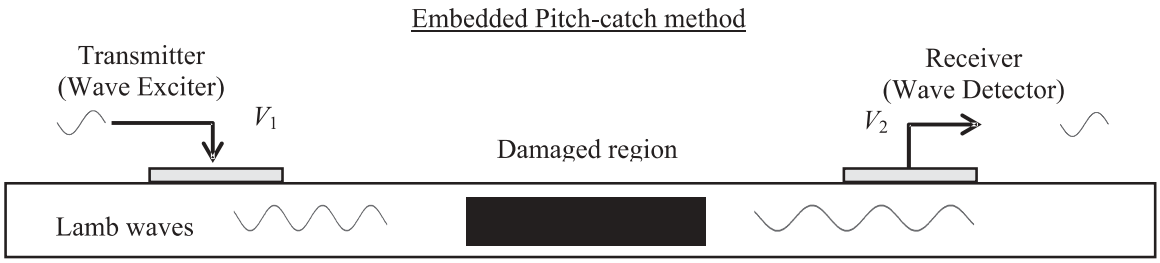

Figure 6. Embedded ultrasonics damage detection techniques with the pitch-catch method.

to generate focused directional waves in metallic specimens. However, the interdigital transducers have a fixed operating frequency that is dictated by the interdigital spacing. Chang and co-workers were among the first to identify the opportunity of using the piezoceramic disk wafers as both transmitters and receivers of Lamb waves. Keilers and Chang (1995) used an array of PWAS affixed to composite plates. Some of these PWAS acted as elastic wave generators, and others acted as structural response receptors. The detection of damage was deduced from the differences in structural-response magnitude over the 0–2 kHz bandwidth. Damage detection criteria based on wave propagation were subsequently developed (Chang, 1998, Wang and Chang, 1999; Osmond et al., 2002; Mal et al., 2003; Wang et al., 2003).

4.3. Crack Detection in Metallic Structures with Embedded Pitch-catch Non-destructive Evaluation

Cracks in metallic structures typically run perpendicular to the wall surface. A fully developed crack will cover the whole thickness (through-the-thickness crack) and will produce a tear of the metallic material. In conventional NDE, metallic-structure cracks are detected with ultrasonic or eddy current probes that have pointwise capabilities. Intensive manual scanning is required for crack detection. The aim of embedded pitch-catch NDE is to detect cracks in metallic structures using guided waves transmitted from one location and received at a different location. The analysis of the change in guided wave shape, phase, and amplitude should yield indications about the crack presence and extension.

Ihn and Chang (2002) and Ihn (2003) presented an embedded pitch-catch method for the detection of cracks in metallic structures using an array of 12 mm diameter piezoceramic disks (Figure 7). A five-count 300 kHz smoothed tone burst applied to the transmitter (T) produced an omnidirectional Lamb wave into the plate. The receiver (R) detects a wave which is modified by the crack presence. The crack was grown through cyclic loading, and measurements were taken at various crack lengths. The readings at zero crack length were taken as the baseline. The scatter wave was defined as the difference between the current received wave and the baseline wave. It was shown that the scatter amplitude increases linearly with the crack length.

Ihn and Chang (2002) and Ihn (2003) applied the same embedded pitch-catch NDE method to detect multisite crack damage in a metallic lap joint specimen (Figure 8). The lap joint contained two rows, each having 19 4.8 mm rivets. A row of 18 embedded transmitters (T) were used to send S_0 Lamb waves to two rows of 18 embedded receivers (R). Constant amplitude cyclic tensile loading for accelerated fatigue testing was used. Multisite crack damage was observed to develop at several locations. The test was interrupted seven times to evaluate the cracks progression (40, 65, 80, 100, 120, and 140 kcycles). Final failure occurred at 160 kcycles. No visual inspection was possible. Crack progression was evaluated with conventional NDE methods (ultrasonic through-the-thickness scan and eddy current probes) as well as with embedded pitch-catch NDE. A damage index based on the cumulative TOF of the 420 kHz S_0 Lamb wave was used.

Figure 9 shows that the probability of detection (POD) of the e-NDE pitch-catch method is comparable with that of conventional ultrasonic and eddy current methods for cracks larger than 5–8 mm. Circles represent embedded pitch-catch NDE; triangles represent eddy currents NDE. To obtain the POD, the different crack events monitored by conventional NDE were ranked from the largest to the smallest crack length and then compared the embedded pitch-catch method, i.e.

$$POD = \frac{SC}{M + 1 - N} \tag{21}$$

where SC is the sum of the crack events recorded by the pitch-catch method, M is the total number of crack events recorded by NDE, and N is the serial event. The embedded pitch-catch NDE was also used for detecting fatigue crack growth in a metallic specimen repaired with a boron-epoxy patch. Good detection of cracks larger than 4–8 mm was observed (Ihn, 2003).

4.4. Crack and Disbond/Delamination Detection in Composite Structures with Embedded Pitch-Catch Non-destructive Evaluation Method

Composite structures are typically resistant to through-the-thickness cracks due to the inherent crack resistance of fiber reinforcement. However, in layered composite structures, cracks can easily propagate parallel to the wall surface, typically at the interface between layers. These cracks can be initiated by fabrication imperfections or low-velocity impact damage; subsequently, they propagate by cyclic fatigue loading. In conventional NDE, composite cracks and delaminations are detected with ultrasonic probes that can

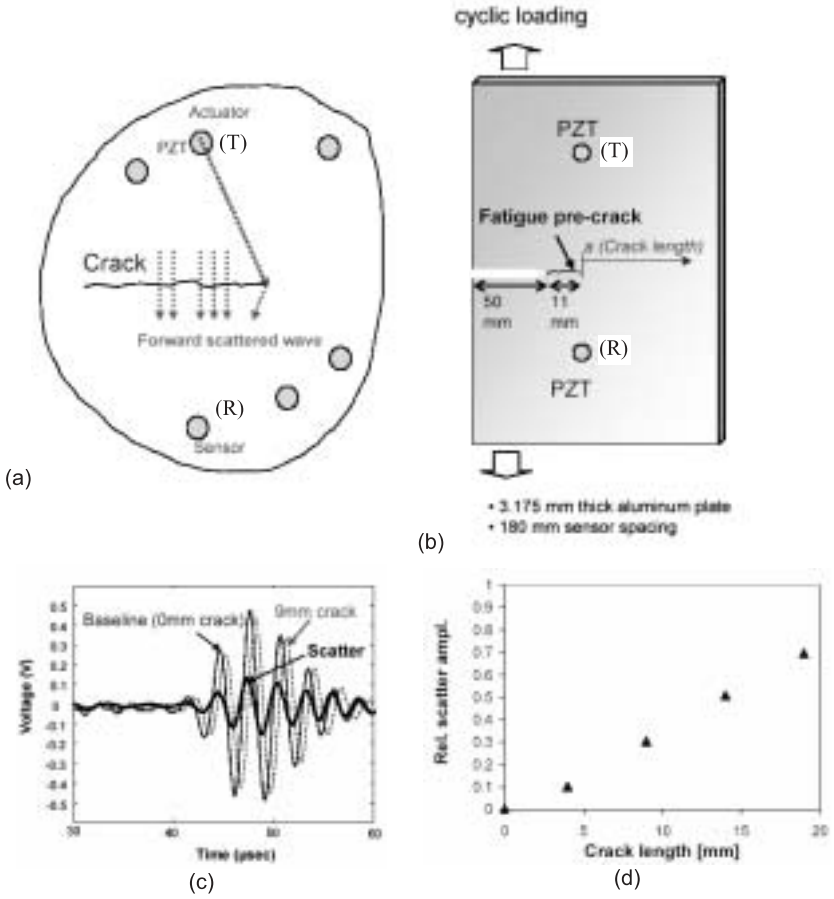

Figure 7. Crack detection in metallic plate with the embedded pitch-catch method: (a) conceptual configuration; (b) experimental setup; (c) received waves and scatter wave; (d) linear variation of scatter amplitude with crack length (Ihn, 2003).

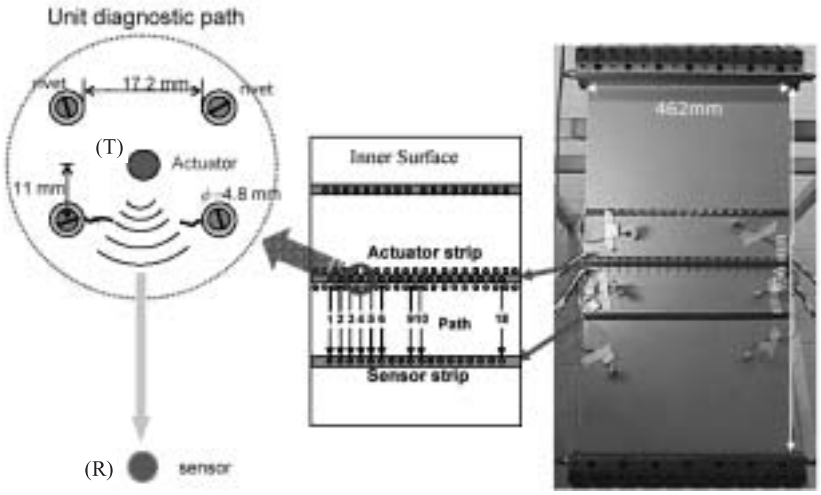

Figure 8. Multisite crack detection in metallic lap joint specimen plate with the embedded pitch-catch method: two rows of 19 rivet holes were monitored using a row of 18 embedded transmitters (T) sending S_0 Lamb-waves to two rows of 18 embedded receivers (R) (Ihn, 2003).

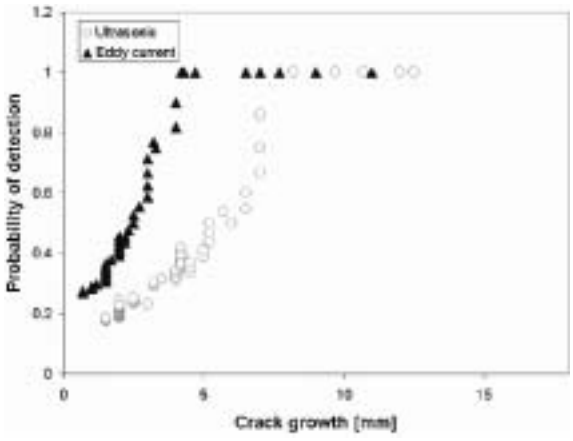

Figure 9. POD of the embedded pitch-catch NDE in comparison with conventional ultrasonics and eddy currents (Ihn, 2003).

sense additional echoes due to through-the-thickness P-waves being reflected by the delamination. Area coverage is achieved with surface scanning (C-scans) using manual means or mechanical gantries. The aim of embedded pitch-catch NDE is to detect cracks and delaminations in composite structures using guided waves transmitted from one location and received at a different location. The disbond/delamination produces signal diffraction and mode conversion that can be analyzed and compared with the pristine signals. Analysis of the change in the guided wave shape, phase, and amplitude should yield indications about the crack presence and its extension. In addition, the sensor network built into the structure can be also used for monitoring low-velocity impact events that may be the cause of composite damage.

Chang (1998) first demonstrated that a network of piezoelectric disks could be embedded in a dielectric film, called the "SMART layer." By emitting controlled diagnostic signals from a piezoelectric disk, the signals could be caught at neighboring piezoelectric disks. The pitch-catch technique was further used by Wang and Chang (1999) to identify impact damage in composite structures. The experimental setup consisted of an array of four piezoelectric disks connected through a selector box to either a signal generator/actuator amplifier or a sensor amplifier/DAQ card. Tone-burst signals were sent from one of the piezoelectric disks and collected at all the other piezoelectric disks, in a round-robin fashion. The tone-burst frequency was swept over the 40–150 kHz range. A_0 Lamb waves traveled in the plate and were scattered by the damage. The signal interpretation consisted of analyzing the short-time Fourier transform (STFT) spectrograms to identify the TOF for each of the six paths possible between the four piezoelectric disks. The resulting TOF measurements were related to the location, size, and orientation of the damage by comparison with TOF values calculated with an analytical model. Detection results obtained with the embedded pitch-catch method compared very well with the specimen X-ray images (Figure 10).

Similarly, Lemistre et al. (1999, 2000) used a network of transmitter–receiver piezoelectric disks (5 mm diameter, 0.1 mm thick) to detect delamination in a composite plate. A 10-cycle 365 kHz tone burst transmitted from one of the piezoelectric disks generated S_0 Lamb waves that were scattered by the damage into A_0 and SH_0 waves through diffraction and mode conversion. The received signals were analyzed with the discrete wavelet transform and compared with the pristine-plate signals. The analysis was performed using simple TOF considerations. No analytical model of the damaged plate was needed. Wavelet transform was also used by Staszewski et al. (1999), Deng et al. (1999), Su and Ye (2004), and others.

Ihn and Chang (2002) and Ihn (2003) used the pitch-catch technique with SMART layer instrumentation to detect disbonds in boron-epoxy composite patch repair of cracks in metallic structures (Figure 11). A SMART layer was embedded between the composite repair layers. A_0 Lamb waves, which are more sensitive to disbond and delaminations, were used. The A_0 Lamb wave frequency was 320 kHz. It was found that the damage index based on A_0 scatter energy was able to correctly detect the disbond presence.

5. Embedded Pulse-echo Method for Crack and Delamination Detection

In conventional NDE, the pulse-echo method has traditionally been used for through-the-thickness testing. For large area inspection, through-the-thickness testing requires manual or mechanical moving of the transducer over the area of interest, which is labor intensive and time-consuming. It seems apparent that guided wave pulse-echo seems more appropriate, since wide coverage could be achieved from a single location.

5.1. Lamb Wave Crack Detection

For crack detection with the pulse-echo method, an appropriate Lamb wave mode must be selected. Giurgiutiu et al. (2003) used finite element simulation to show that the S_0 Lamb waves can give much better reflections from through-the-thickness cracks than the A_0 Lamb waves (Figure 12). This effect can be attributed to S_0 being (a) better reflected from the crack and (b) much less dispersive. The first item gives a strong signal, while the second ensures that the wave packet is compact and easy to interpret.

The use of guided waves for crack detection has found an immediate application in long and uniform structures, such as pipes, tubing, and cables. The advantage of using guided waves is immediately apparent. Conventional through-the-thickness testing requires large pipe areas to be minutely inspected. In addition, access to the outside pipe surface requires removal of the insulation and then reinstallation of the insulation after the tests. Using guided waves, a probe can be applied to the pipe at only one location, from which a considerable length of the pipe can be inspected. The insulation is only removed at the location where the probe is applied. Special probes are available for guided wave pipe inspection. Alleyne et al. (2001) developed a "comb" array probe which surrounds the pipe. Kwun and Bartels (1998) and Kwun et al. (2002) developed an electromagnetically coupled transducer for SH guided waves using a portable

(a)

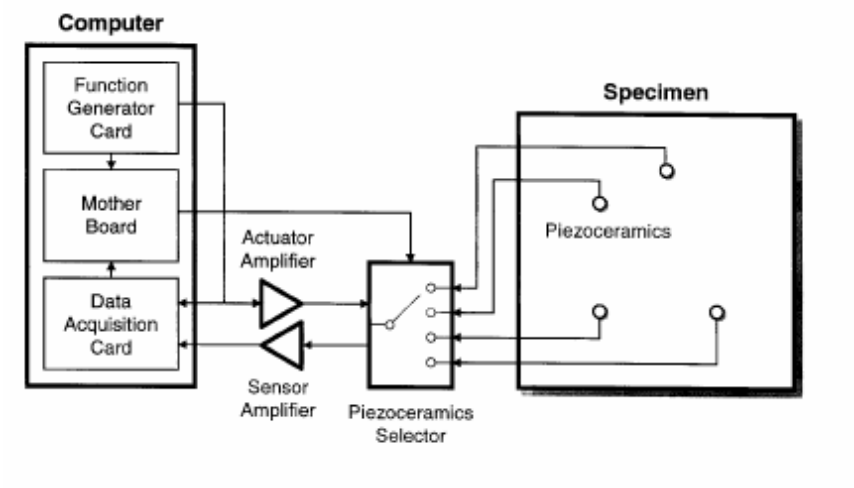

(b)

$[0_4/90_4]_s$

	a	b	χ^2
Estimated	1.4	0.6	2°
Real	1.2	0.5	0°

Unit: inch

$[0_2/45_2/-45_2/90_2]_s$

	a	b	χ^2
Estimated	0.9	0.5	27°
Real	0.8	0.4	32°

a: semi-major axis of the damage.
b: semi-minor axis of the damage.
χ^2: angle between semi-major axis and 0° fiber direction.

Figure 10. Impact damage identification in composite structures using the embedded pitch-catch method: (a) experimental schematic diagram; (b) picture of the panel showing the "real damage" detected by X-rays, and the "estimated damage" detected by the embedded pitch-catch method. The locations of the four piezoelectric disks ("PZT") are also shown (Wang and Chang, 1999).

coil and a nickel foil affixed to the structure. Rose et al. (1994) studied the use of guided waves for the inspection of nuclear steam generator tubing. Reflections from circumferential cracks were obtained. Alleyne et al. (2001) used guided waves to detect circumferential cracks and corrosion in steel pipes. The properties of axial-symmetric and non-axial-symmetric modes were used. For circumferential cracks, it was found that the reflection coefficient is directly proportional to the circumferential extent. Thus, the reflection coefficient of a half wall thickness notch with a circumferential extent of half a pipe diameter (16% of the pipe circumference) is approximately 5% (–26 dB). This detection sensitivity (40 dB signal-to-coherent-noise ratio) was found satisfactory for most applications. The detection of longitudinal cracks in pipes was achieved by Luo et al. (2003) using electromagnetically coupled SH (torsional) waves. Light et al. (2002) used the same method to detect through-the-thickness cracks in plates. Rizzo and Lanza di Scaldia (2004) used guided waves to detect crack in tendons and suspension cables.

5.2. Crack Detection with Embedded Pulse-echo Method

The embedded pulse echo method follows the general principles of conventional Lamb wave NDE. A PWAS transducer attached to the structure acts as both transmitter and detector of guided Lamb waves traveling in the structure. The wave sent by the PWAS is partially reflected at the crack. The echo is captured at the same PWAS acting as

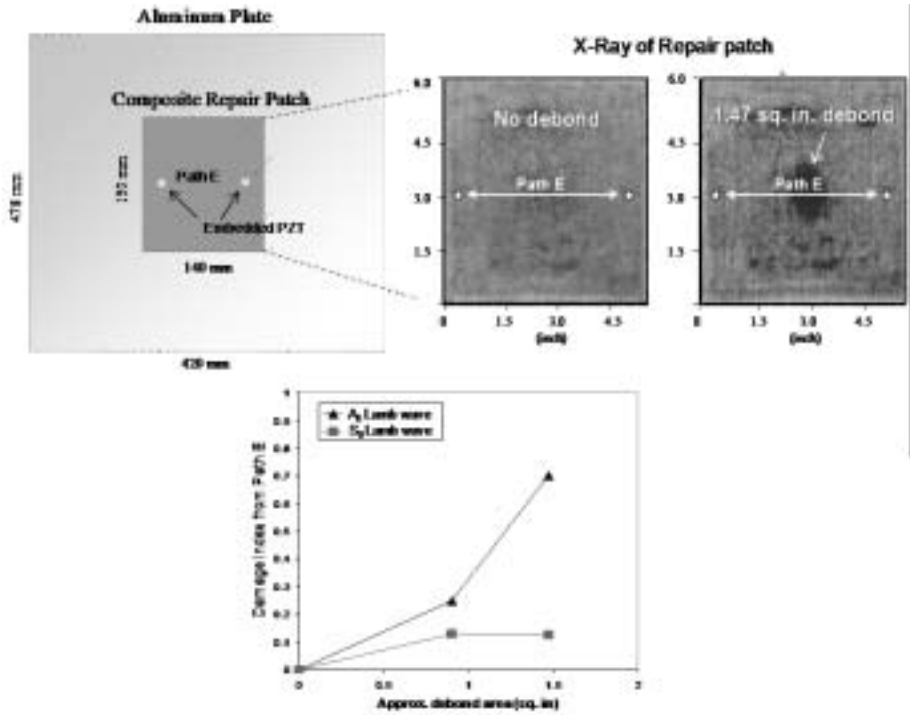

Figure 11. Embedded pitch-catch NDE for disbond detection of composite repairs of metallic structures (Ihn, 2003).

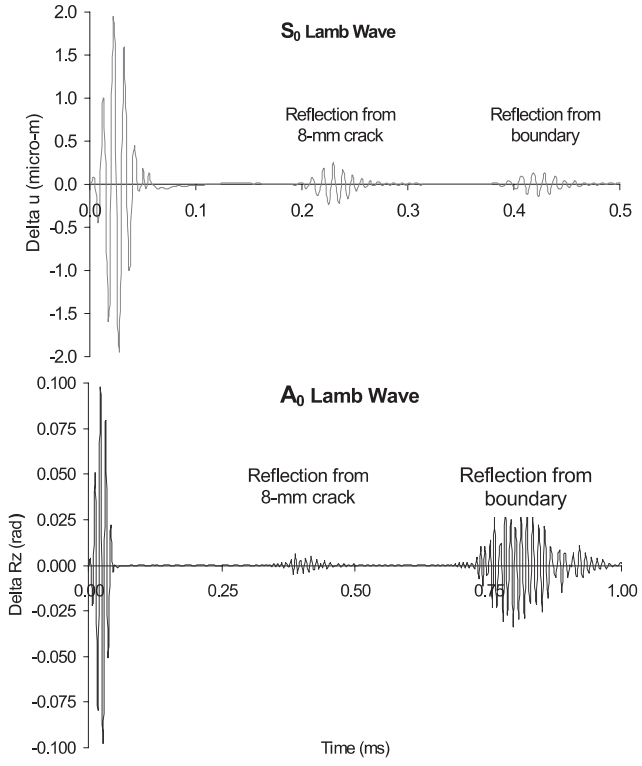

Figure 12. Finite element simulation indicates that S_0 Lamb waves can give better crack reflections than the A_0 Lamb waves (Giurgiutiu et al., 2003).

receiver (Figure 13). For the method to be successful, it is important that a low-dispersion Lamb wave is used. The selection of such a wave, e.g. the S_0 mode, is achieved through the Lamb wave tuning methods (Giurgiutiu, 2003).

Moetakef et al. (1996) studied Lamb wave generation in metallic beams by piezoceramic wafers with interdigital electrodes. This approach, bearing on the SAW technology, ensures excitation of the guided waves having the half-wavelength equal to the interdigital spacing. The transmitted signal was enhanced by phasing the excitation to individual electrodes proportional to the electrode spacing. For detection, single-electrode probes of half-wavelength width were used (Figure 14). Successful detection of echoes from notches was also reported.

Diaz Valdes and Soutis (2002) studied the detection of delaminations in a composite beam using the embedded pulse-echo method with low-frequency A_0 Lamb waves. Figure 15(a) shows the experimental setup. Rectangular PWAS (20×5 mm^2) were used with the length oriented along the beam axis. This ensures that Lamb waves were predominantly excited along the beam length. Two PWAS were used: one as transmitter (actuator), the other as receiver (sensor). A 5.5 cycle 15 kHz Hanning smoothed tone burst was applied to the transmitter PWAS. Figure 15(b) shows the signal recorded in the pristine beam. The initial bang and the reflection from the end of the beam are apparent. Then, a delamination was generated in the composite beam using a scalpel blade. The size of the delamination was progressively increased, as indicated in Figure 15(c). The presence of the delamination crack produced an additional echo, as shown in Figure 15(d). This work was extended to composite plates by Diamanti et al. (2002).

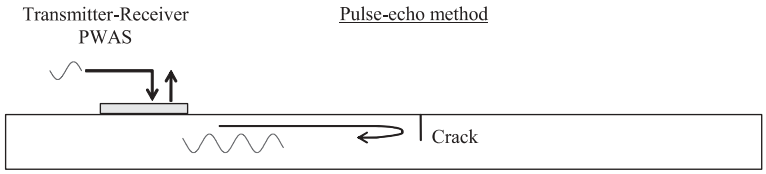

Figure 13. Principles of embedded ultrasonics damage detection with the pulse-echo method.

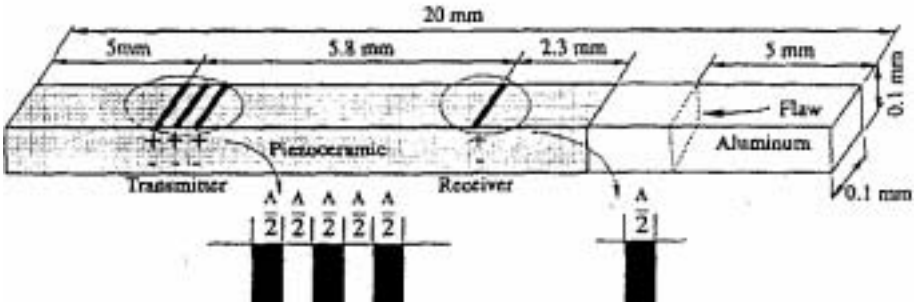

Figure 14. Interdigital transmitter and single electrode receiver used for damage detection in an aluminum beam (Moetakef et al., 1996).

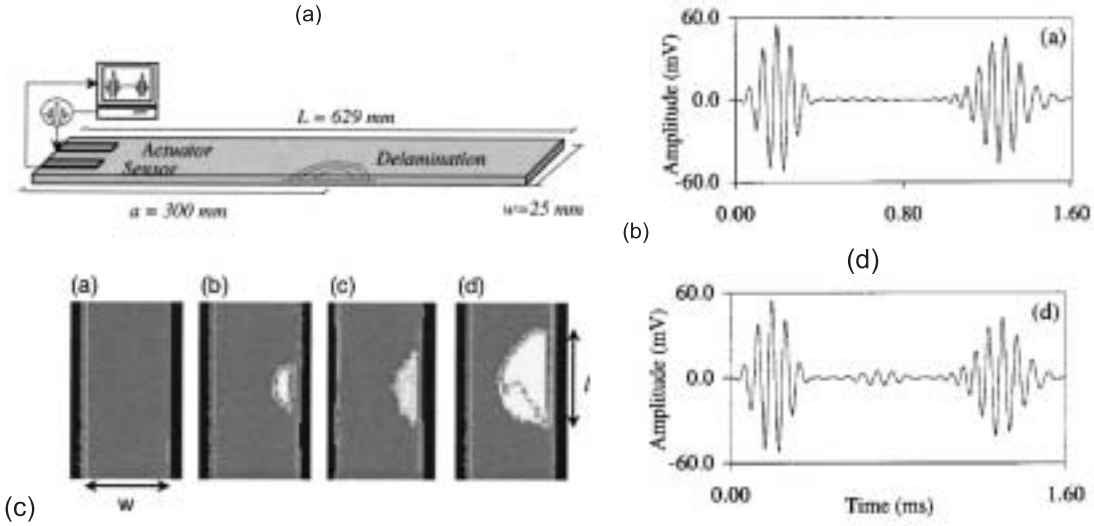

Figure 15. Detection of delaminations with the embedded pulse-echo method: (a) experimental setup; (b) signals in the pristine specimen show only reflections from the beam end; (c) through-the-thickness C-scans of the specimen with conventional ultrasonics; (d) signal in damaged specimen shows additional echo from the delamination crack.

Osmond et al. (2002) used the embedded pulse-echo method to detect damage in the foam core of a sandwich plate with glass fiber skins. The damage was simulated by a hole in the foam. Low-frequency A_0 Lamb waves (10 and 20 kHz) were used. It was shown that damage location and intensity can be deduced from the echo analysis without an analytical model of the damaged plate. Barnoncel et al. (2003) used the same method to detect real impact damages.

For detection of through-the-thickness cracks in metallic specimens, higher-frequency S_0 Lamb waves are required, such that the wavelength is sufficiently smaller than the crack. Figure 16 presents crack detection experiments performed with an embedded PWAS on a metallic aircraft panel. The panel has a typical aircraft construction: vertical splice joint and horizontal stiffeners (the splice is only partially shown at the left of the picture). The top panel is pris-

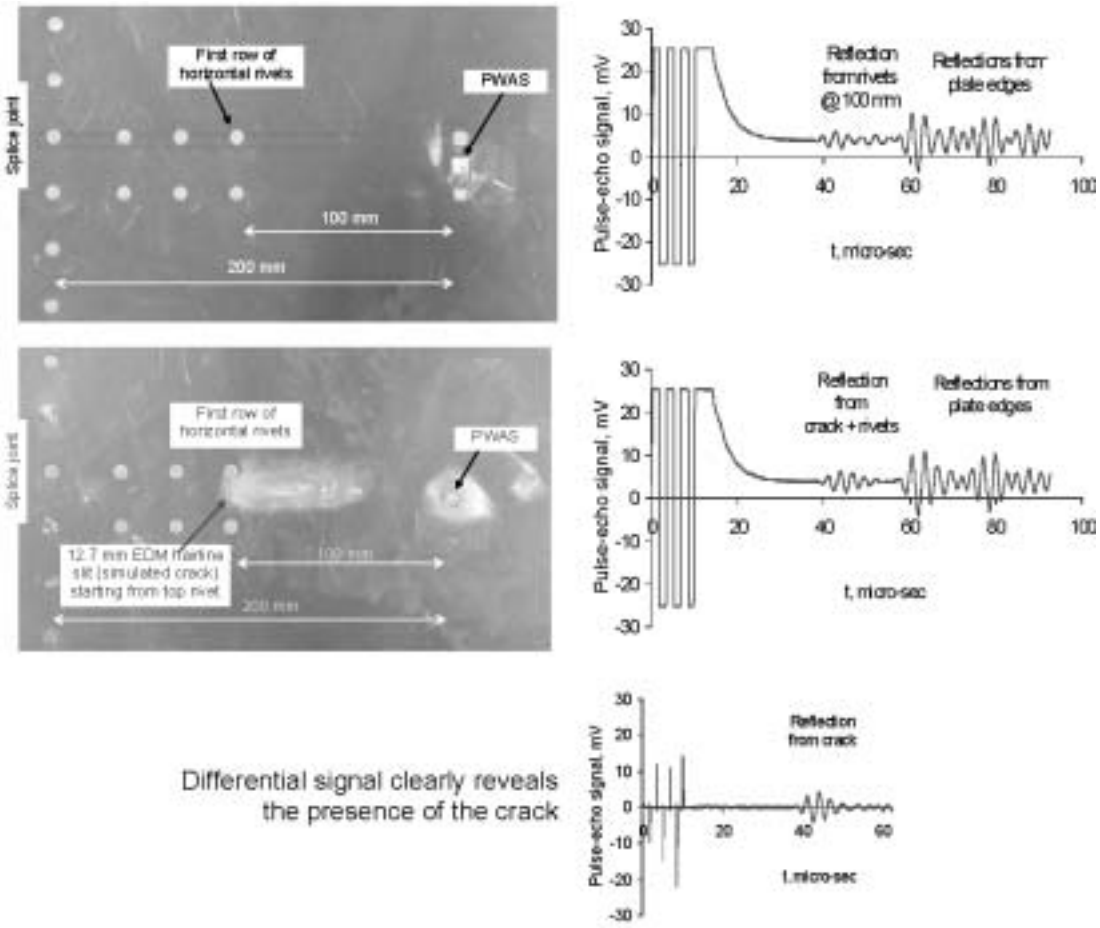

Figure 16. Crack detection experiments on an aircraft panel: the left column represents specimens (1 mm 2025 T3); the right column represents the pulse-echo signals. The last cell in the right column shows the crack detection through the differential signal method.

tine, while the bottom panel has a simulated through-the-thickness crack (12.7 mm hairline slit) emanating from the first rivet hole in the top horizontal row. One PWAS was installed on each panel at 100 mm from the first rivet (200 mm from the splice joint). Adjacent to each photograph are the pulse-echo signals. For the pristine panel, the signal contains reflections from the splice joint and backscatter from the rivet holes located at the beginning of the horizontal row. The echoes from the structural splice start to arrive at approximately 60 μs, while the backscatter from the rivets is visible at around 42 μs. For the panel with a simulated crack, similar signal features appear; however, the feature at the 42 μs position is somehow stronger due to the presence of the crack. Indeed, the signal feature at 42 μs corresponds to the superposed signals from the rivets and from the crack. The detection of the crack seems particularly difficult because the echoes from the crack are mixed with the backscatter from the collocated rivets.

This difficulty can be easily resolved in an SHM situation, in which historical signal records are available. Thus, one can apply the differential signal method, i.e. subtract the "pristine" signal from the "damage" signal. Such a situation of using archived signals is typical of health monitoring systems. When the two signals were subtracted, the result presented in the last row of Figure 16 was obtained. This differential signal shows a "loud and clear" echo due entirely to the crack. The echo, marked "reflection from the crack" is centered at 42 μs, which corresponds to a TOF of 37 μs as measured from the center of the "initial bang". This value correlates very well with a total travel from the PWAS to the crack at the S_0 mode speed $c_{S_0} = 5.4$ mm μs^{-1}. This simple experiment demonstrates the capability of embedded PWAS to detect structural cracks. However, one problem remains: this one-PWAS detection lacks directionality. The detected crack can be anywhere on a 100 mm radius. To obtain directionality of detection, a PWAS phased array can be used, as shown in the next section.

6. Embedded Phase Arrays for Large Area Imaging

Real-time phased-array systems have become very popular in NDE practice. Krautkramer (2002) offers a product line of phased-array transducers for the inspection of very thick specimens, and for the sidewise inspection of thick slabs, etc., with P-waves (Figure 17). For Rayleigh and Lamb waves, Deutsch et al. (1997, 1998, 1999) developed a

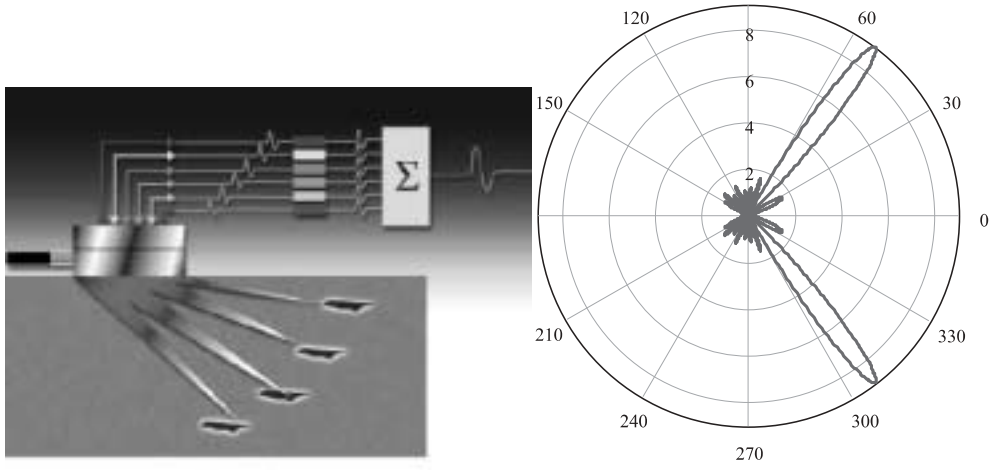

Figure 17. (a) Conventional phased-array ultrasonic probe (Krautkramer, 2002). (b) Illustration of phased-array principle.

phased-array self-focusing method, by which the delay times are adjusted to focus the beam exactly on the defect. Schwartz et al. (1999) proposed a Lamb wave ultrasonic tomography imaging system for aircraft structural health assessment. The acquisition and processing of Lamb wave data uses the image reconstruction method and is based on algorithms developed for cross-borehole tomography. The transducer geometry consists of parallel arrays of transmitters–receivers. The simulated damage was a circular defect with a 2.5 mm diameter in an aluminum plate. The results showed that the method could accurately determine the dimension, shape, and location of defect by reconstructing an area of 30.5×30.5 cm^2.

Moulin et al. (2003) studied the feasibility of inducing beam steering with embedded rectangular PWAS. A three-element array mounted on a composite plate was used as transmitter of somehow directional beams of S_0 Lamb waves, while peripherally placed PWAS were used as receivers. Changes in the signal amplitudes due to damage were observed. Beam steering studies were also carried out by Sundaraman and Adams (2002), Purekar and Pines (2003), and others.

Giurgiutiu and Bao (2002) developed a PWAS phased-array technique, the EUSR. Its principle of operation is derived from two general concepts:

(1) the generation of tuned guided Lamb wave with PWAS;
(2) the principles of conventional phased-array radar.

The EUSR approach is different from the conventional phased array approach in two aspects:

(1) it uses structurally-embedded PWAS transducers;
(2) it works in virtual time, not in real time.

Of these two items, the latter is very important for SHM, because it allows the phased-array benefits without the drawback of real-time multichannel phased excitation equipment. Whereas real-time phased-array transducers require heavy and complex multichannel phased excitation equipment, the virtual-time approach adopted by the EUSR method can be carried out with only one channel and very simple equipment (Figure 18). On the investigated structure, the EUSR method captures and stores an array of elemental signals. In a round-robin fashion, one PWAS is activated as transmitter, while all the PWAS, including the transmitter, act as receivers. The activated sensor acts in pulse-echo mode, i.e. as both transmitter and receiver; the other sensors act as passive sensors. Thus, a matrix of $M \times M$ elemental signals is generated. In the post-processing phase, the elemental signals are assembled into the synthetic beamforming response using the synthetic beamformer algorithm.

6.1. Phase Array Principles Used in the Embedded Ultrasonic Structural Radar

The principles of conventional phased-array radar (Silvia, 1987) are applied to the EUSR algorithm assuming a uniform linear array of M transmitter/receivers PWAS, where each PWAS acts as a pointwise omnidirectional source/sink. The PWAS in the array are spaced at the distance $d = \lambda / 2$, which is assumed much smaller than the distance r to a generic, far-distance point, P. Since $d << r$, the rays joining the sensors with the point P can be assimilated with a parallel fascicle, of angle ϕ. Therefore, for the mth PWAS, the distance will be shortened by $m(d \cos\phi)$. If all the PWAS are fired simultaneously, the signal from the mth PWAS will arrive at P quicker by $\Delta_m(\phi) = m(d \cos\phi) / c$. Yet, if the PWAS are not fired simultaneously, but with some individual delays, δ_m, $m = 0, 1, \ldots, M-1$, then the total signal received at point P will be

$$s_{\mathrm{P}}(t) = \frac{1}{\sqrt{r}} \sum_{m=0}^{M-1} s_{\mathrm{T}}\left(t - \frac{r}{c} + \Delta_m(\phi) - \delta_m\right), \tag{22}$$

where $1/\sqrt{r}$ represents the decrease in the wave amplitude due to the omnidirectional two-dimensional radiation, and

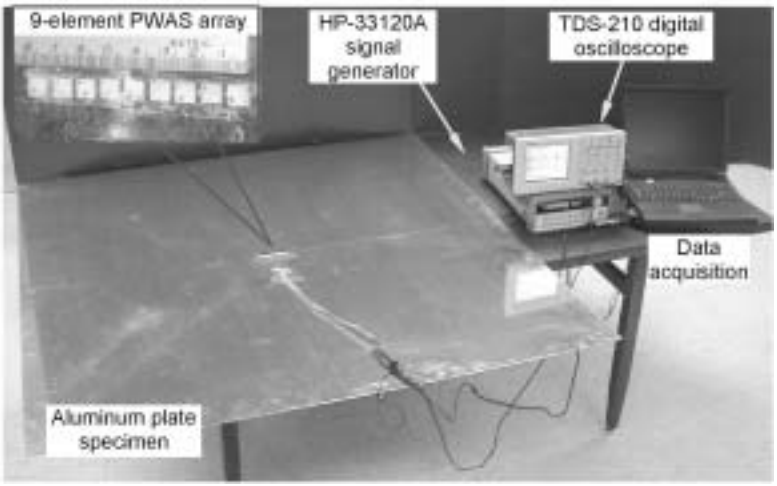

Figure 18. Experimental setup for the EUSR method (Giurgiutiu and Bao, 2002).

r / c is the delay due to the travel distance between the reference PWAS ($m = 0$) and the point P. (Wave-energy conservation with no dissipation is assumed.)

Transmitter beamforming is achieved by making $\delta_m = m\Delta(\phi)$. Equation (22) becomes

$$s_P(t) = M \cdot \frac{1}{\sqrt{r}} s_T\left(t - \frac{r}{c}\right). \tag{23}$$

Equation (23) shows an M times increase in the signal strength with respect to a single PWAS due to the constructive interference of all the PWAS signals when the geometric delay, Δ_m, and the firing delay, δ_m, coincide. Since $\Delta_m = md\cos(\phi) / c$, we can write $\delta_m = md\cos(\phi_0) / c$ which indicates that beamforming will take place when $\cos(\phi) = \cos(\phi_0)$, i.e. at angles $\phi = \pm\phi_0$.

Receiver beamforming is achieved in a similar way. We synchronize the signals received from a point P at azimuth ϕ_0, by using the delays

$$\delta_m(\phi_o) = m\frac{d}{c}\cos(\phi_0). \tag{24}$$

The pulse-echo method consists of combining the transmitter beamforming with the receiver beamforming, and then we steer the interrogation beam at the target existing at azimuth ϕ_0 and range R. At the target, the signal is backscattered with a backscatter coefficient, A. Hence, the echo signal is

$$s_R(t) = \frac{A \cdot M^2}{R} \sum_{m=0}^{M-1} s_T\left(t - \frac{2R}{c}\right). \tag{25}$$

Then, the target range R can be calculated from the echo TOF $\tau = 2R / c$. By two-dimensionally plotting the reconstructed signals obtained for incremental ϕ_0 values, one can map a complete half-plane into an image indicating the position of the target.

6.2. Experimental Results with the EUSR Method

EUSR experiments were conducted in the Laboratory for Adaptive Materials and Smart Structures (LAMSS) at the University of South Carolina. The experimental setup is presented in Figure 18. The specimens consists of a 1 mm thick aluminum square plate (1220×1200 mm^2) with a PWAS array in the middle (nine APC 850 piezoceramic wafers, 0.2 mm thick, 7×7 mm^2, 9 mm spacing). One specimen had a simulated broadside crack ($\phi_0 = 90^o$, R = 305 mm), the other an offside crack ($\phi_0 = 136.3^o$, R = 409 mm). The simulated cracks were 20 mm long, 0.127 mm wide. The excitation was a three-count smoothed tone burst of 300 kHz S_0 Lamb waves. In a round-robin fashion, a total of $9 \times 9 = 81$ elemental signals were collected. Figure 19(a) shows the location and size of the simulated crack (narrow slit) situated broadside with respect to the phased array. Figure 19(b) shows the imaging of the crack on the EUSR GUI and the reconstructed pulse-echo signal (A-scan). The signal reconstruction and the crack imaging were performed in virtual time by applying the EUSR algorithm to the set of 81 elemental signals. By stepping the scanning beam through the interval 0^o to 180^o, a complete scan of the plate upper half was obtained with the crack location clearly defined by a pronounced gray-scale change (Figure19(b)). The A-scan signal can be used for precise identification of the crack location using the TOF $\tau = 112.4$ μs and the group velocity $c_{g\_S0} = 5.440$ mm μs^{-1}, which yields R = 305.7 mm, i.e. a mere 0.2% from the actual value ($\phi_0 = 90^o$, R = 305 mm). Similar results were obtained for the offside crack (Figures 19(c) and (d)), in spite of the fact that the offside crack did not return a direct echo, but only diffractions from the crack tips (as shown in Figure19(c), the ultrasonic beam is deflected away from the phased array, but the crack tips generate diffraction signals that are felt at the phased array).

In order to verify the effect of curvature, the thin aluminum plate was temporarily bent into cylindrical shapes using thin wire ropes and tightening screws. The realized curvatures were related to the shortening of the chord with

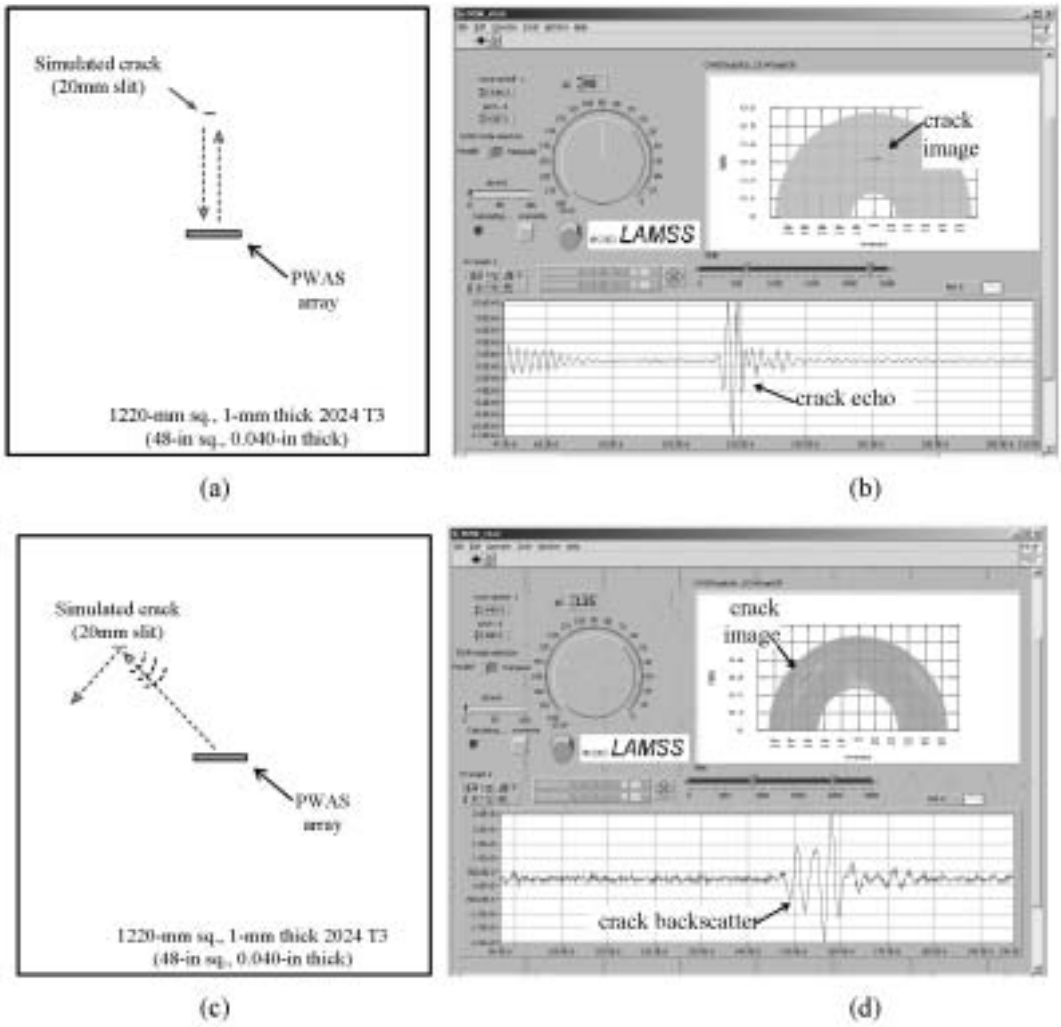

Figure 19. Crack detection in a flat plate: (a) location and size of simulated broadside crack; (b) imaging and echo of broadside crack in the EUSR algorithm; (c) location and size of simulated offside crack; (b) imaging and echo of offside crack in the EUSR algorithm.

respect to the original flat length. After curving, the original flat length, L, became the circular arc, while the shorted wire rope became the chord, $c = 2R\sin(L/2R)$. The difference between the original length, L, and the shortened length, c, was denoted by ΔL. By varying ΔL, we were able to vary R according to the relation

$$R = (L - \Delta L)/[2\sin(L/2R)]. \tag{26}$$

Shortenings of values ΔL = 5, 10, 15, and 20 mm corresponding to curvature values R = 3.90, 2.75, 2.24, and 1.95 m were used. These curvatures were applied in two directions. One direction was with the chord parallel to the PWAS array, while the other was with the chord perpendicular to the PWAS array. In both cases, good detection of the simulated crack was observed (Giurgiutiu et al. 2004).

7. Other Techniques

Other interesting techniques for performing active SHM include, among others, the time reversal method and the migration technique.

7.1. Time Reversal Method

The time reversal method was developed by Fink (1992) in connection with the pitch-catch NDE method. The signal sent by the transmitter arrives at the receiver after being modified by the medium in which it travels. If the received signal is time reversed and sent back from the receiver to the transmitter, the effect of the medium is also reversed. This reversal is quite spectacular in the case of dispersive Lamb waves. In a series of remarkable experiments, Ing and Fink (1998) showed that the extensive dispersion of certain Lamb wave modes can be almost completely compensated through

the time reversal method. Deutsch et al. (1997) also used to concept of reversing the reflected waves in order to focus a linear array of conventional ultrasonic transducers transmitting Rayleigh and Lamb waves. The time reversal method has proven especially useful in ultrasonic imaging of difficult media (Berryman et al., 2002).

In SHM, the time reversal method has been recently reported by several authors. Wang et al. (2003) used the time reversal method on an aluminum plate. Sohn et al. (2004a) and Park et al. (2004) used the time reversal method to detect damage in composite panels. Their approach uses the assumption that "because the time reversibility of waves is fundamentally based on the linear reciprocity of the system, this linear reciprocity and the time reversal break down if there exist any source of wave distortion due to wave scattering along the wave path. Therefore, by comparing the discrepancy between the original input signal and the reconstructed signal, damage could be detected." This approach seems to remove the need for a historical baseline, which is inherent in other SHM methods. In addition, the method uses wavelet signal generation and processing to enhance the time reversal process in the case of multimode Lamb wave propagation.

7.2. Migration Technique

The migration technique is a signal processing method that originated in geophysical acoustics. In geophysical exploration, a small explosion is created on the Earth's surface, which generates wave traveling in the Earth's interior and on its surface. A number of geophones are used to record both the initial bang and the waves reflected from the various inhomogeneities in the Earth interior. The migration technique attempts to image the subsurface reflectors by moving ("migrating") the recorded wave field to the actual spatial locations of these reflectors in the Earth's interior. The process back-propagates the recorded waves by systematically solving the wave equation as time-dependent boundary value problems based on Huygens' principle.

Lin and Yuan (2001b, 2001c, 2005) adapted the migration technique to the SHM of damage in plates. Both finite difference simulations and experimental results obtained on an aluminum plate were presented. The antisymmetric plate waves were modeled with Midlin's plate theory and the wave propagation solution was calculated with a finite difference algorithm. This finite difference method migrates backwards the waves diffracted by the damage to identify the damage location and extend. A linear array of sparsely spaced PWAS was used to detect crack damage using the migration technique. Nine piezoelectric disks were mounted at 25 mm (1 inch) interval across a metallic plate and used in turn as transmitters and receivers of antisymmetric plate waves in a round-robin fashion. The damage was simulated in the form of an arc-shaped through-the-thickness slit (1.1 mm wide, 12.5 mm radius) placed at 150 mm (6 inches) from the transducers. The transmitter transducer creates a wave front that is scattered by the damage and comes back to the receiver transducers where it is recorded in digital format. In processing the experimental data, the migration time-step was taken equal to the sampling interval of the analog-to-digital (A/D) converter. At each time-step, the received waves are migrated (back-propagated) towards the damage location. Applying migration to each time section gives an image of the plate based on a single transmitter. An enhanced image is obtained by adding (stacking) the individual contributions of all the transmitters in the round-robin process. This is the pre-stack migration method. As an alternative, the stacking can be done first (with appropriate synchronization of the individual signals), and the migration done second. This is the post-stack migration method. The post-stack migration is less computationally intensive, but the pre-stack migration is more powerful in increasing the signal-to-noise ratio.

8. Conclusions and Further Work

In this paper, an emerging new technology has been discussed: embedded ultrasonic NDE. This emerging technology is enabled by the use of embeddable ultrasonic transducers consisting of thin piezoelectric wafers that can be permanently attached to metallic and composite structures. For lack of a better term, Giurgiutiu et al. (2000) have called these embeddable transducers PWAS. The embedded ultrasonic technology enables active SHM, i.e. the on-demand interrogation of the structure, to determine its current state of health and predict the remaining life.

After reviewing the guided wave theory in plate, tube, and shell structures, we introduced the embeddable PWAS transducers. The PWAS piezoelectric properties (actuation and sensing) have been presented in connection with Lamb wave excitation and detection. It is shown analytically and verified experimentally that Lamb wave mode tuning can be achieved by the judicious combination of PWAS dimensions, frequency values, and Lamb wave mode characteristics. For example, the A_0 and S_0 Lamb modes could be separately tuned by using the same PWAS installation but different frequency bands.

The embedded pitch-catch method was discussed in the context of detecting through-the-thickness fatigue cracks in metallic structures and delamination and disbond cracks in composite and other bonded structures. Then, the embedded pitch-catch method was considered, again in metallic structures and in composites. Finally, the embedded phased array method was presented, with special attention to the EUSR. Examples of crack detection and imaging were provided for both flat and curved metallic plates. Other methods, such as the time reversal method and the migration techniques, have also been discussed.

Although remarkable progress has been made in the embedded ultrasonic NDE development, considerable work remains to be done. To increase the acceptance of this emerging technology, the refining of the theoretical analysis and calibration against well-planned experiments is needed. However, to deploy e-NDE techniques to in-service structures, several hurdles have still to be overcome. In particular, the operational and environmental variations of the monitored structure need to be addressed. The NDE techniques presented above perform damage diagnosis through pattern comparison of a test signal with a baseline signal. This type of simple pattern comparison may be vulnerable to undesired changes of signals due to varying operational and environmental conditions of the structure such as temperature variation, humidity, etc. Several authors have addressed this aspect (e.g. Mason, 2002; Sohn et al., 2004b; and others).

Further, a better understanding of the micromechanical coupling between PWAS and structure for various Lamb modes must be achieved. In addition, the behavior of the bonding layer between the PWAS and the structure must be clarified, such that predictable and repeatable results are achieved. The durability of this bond under extended environmental exposure must be determined. Last, but not least, the signal analysis methods must be developed to achieve probability of detection values at least comparable with that of conventional NDE methods.

Acknowledgments

The financial support of the Air Force Research Laboratory, Materials and Manufacturing Directorate, NDE Branch, under Universal Technology Corporation contract F33615-03-D-5204; Air Force Office of Scientific Research grant FA9550-04-0085, Capt. Clark Allred, PhD, program manager; National Science Foundation award CMS 0408578, Dr. Shih Chi Liu, program director, are gratefully acknowledged. Special thanks are expressed to Professor Fu-Kuo Chang and Dr. Jeong-Beom Ihn for their invaluable help with documentary material and constructive comments for the writing of Sections 4.3 and 4.4. Thanks are extended to all the authors that have kindly provided electronic files of their papers that greatly facilitated the writing of this review paper.

References

Achenbach, J. D., 1973, *Wave Propagation in Elastic Solids*, Elsevier, Amsterdam.

Alleyne, D. N. and Cawley, P., 1992, "The Interaction of Lamb Waves with Defects," *IEEE Transactions on Ultrasonics, Ferroelectrics, and Frequency Control*, Vol. 39, 381–397.

Alleyne, D. N., Pavlakovic, B., Lowe, M. J. S., and Cawley, P., 2001, "Rapid, Long-range Inspection of Chemical Plant Pipework Using Guided Waves," *Review of Progress in QNDE*, Vol. 20, 180–187.

Associated Press (AP), 2003, "NASA To Add Sensors to Shuttle; New Wing Device to Detect Any Damage from Debris," December 11, http://msnbc.msn.com/id/3685882/.

Barnoncel, D., Osmont, D., and Dupont, M., 2003, "Health Monitoring of Sandwich Plates with Real Impact Damages Using PZT Devices," in *Structural Health Monitoring 2003*, Fu-Kuo Chang, ed., DEStech Pub, 871–878.

Berryman, J., Borcea, L., Papanicolaou, G., and Tsogka, C., 2002, "Statistically Stable Ultrasonic Imaging in Random Media," *Journal of the Acoustical Society of America*, Vol. 112, 1509–1522.

Blitz, J. and Simpson, G., 1996, *Ultrasonic Methods of Non-destructive Testing,* Chapman and Hall, London.

Boller, C., Biemans, C., Staszewski, W., Worden, K., and Tomlinson, G., 1999, "Structural Damage Monitoring Based on an Actuator–Sensor System," in *Proceedings of SPIE Smart Structures and Integrated Systems Conference*, Newport, CA.

Butterworth-Hayes, P., 2003, "Europe Seeks 7E7 Work," *Aerospace America*, November, American Institute for Aeronautics and Astronautics, 4–6.

Chang, F-K., 1995, "Built-in Damage Diagnostics for Composite Structures," in *Proceedings of the 10th International Conference on Composite Structures (ICCM-10)*, Vol. 5, Whistler, BC, Canada, August 14–18, 283–289.

Chang, F-K., 1998, "Manufacturing and Design of Built-in Diagnostics for Composite Structures," in *Proceedings of the 52nd Meeting of the Society for Machinery Failure Prevention Technology*, Virginia Beach, VA, March 30–April 3.

Chona, R., Suh, C. S., and Rabroker, G. A., 2003, "Characterizing Defects in Multilayer Materials Using Guided Ultrasonic Waves," *Optics and Lasers in Engineering*, Vol. 40, 371–378.

Crawley, E. F. and Anderson, E. H., 1990, "Detailed Models of Piezoceramic Actuation of Beams," *Journal of Intelligent Material Systems and Structures*, Vol. 1, No. 1, 4–25.

Crawley, E. F. and de Luis, J., 1987, "Use of Piezoelectric Actuators as Elements of Intelligent Structures," *AIAA Journal*, Vol. 25, No. 10, 1373–1385.

Dalton, R. P., Cawley, P., and Lowe, M. J., 2001, "The Potential of Guided Waves for Monitoring Large Areas of Metallic Aircraft Fuselage Structure," *Journal of Nondestructive Evaluation*, Vol. 20, 29–45.

Deng, X., Wang, Q., and Giurgiutiu, V., 1999, "Structural Health Monitoring Using Active Sensors and Wavelet Transforms," in *Proceedings of the SPIE 6th Annual International Symposium on Smart Structures and Materials*, Newport Beach, CA.

Deutsch, W. A. K., Cheng, A., and Achenbach, J. D., 1997, "Self-focusing of Rayleigh Waves and Lamb Waves with a Linear Phased Array," *Research in Nondestructive Evaluation*, Vol. 9, No. 2, 81–95.

Deutsch, W. A. K., Deutsch, K., Cheng, A., and Achenbach, J. D., 1998, "Defect Detection with Rayleigh and Lamb Waves Generated by a Self-focusing Phased Array," *NDT.net*, Vol. 3, No. 12, 1–6.

Deutsch, W. A. K., Cheng, A., and Achenbach, J. D., 1999, "Focusing of Rayleigh Waves: Simulation and Experiments," *IEEE Transactions on Ultrasonics, Ferroelectrics, and Frequency Control*, Vol. 46, No. 2, 333–340.

Diamanti, K., Hodgkinson, J. M., and Soutis, C., 2002, "Damage Detection of Composite Laminates Using PZT Generated Lamb Waves," in *Proceedings of the 1st European Workshop on Structural Health Monitoring*, July 10–12, Paris, France, 398–405.

Diaz Valdes, S. H. and Soutis C., 2002, "Real-time Non-destructive Evaluation of Fiber Composite Laminates Using Low-frequency Lamb Waves," *Journal of the Acoustical Society of America,* Vol. 111, No. 5, 2026–2033.

Duke, J. C. Jr, 1988, *Acousto-Ultrasonics – Theory and Applications*, Plenum Press, New York.

Dupont, M., Osmont, R., Gouyon, R., and Balageas, D. L., 2000, "Permanent Monitoring of Damage Impacts by a Piezoelectric Sensor Based Integrated System," in *Structural Health Monitoring 2000*, Technomic, Lancaster, PA, 561–570.

Fink, M., 1992, "Time Reversal of Ultrasonic Fields – Part I: Basic Principles," *IEEE Transactions on Ultrasonics, Ferroelectrics, and Frequency Control*, Vol. 39, No. 5, 555–566.

Gachagan, A., Hayward, G., McNab, A., Reynolds, P., Pierce, S., Philip, W., and Culshaw, B., 1999, "Generation and Reception of Ultrasonic Guided Waves in Composite Plates Using Comformable Piezoelectric Transmitters and Optical-fiber Detectors," *IEEE Transactions on Ultrasonics, Ferroelectrics, and Frequency Control*, Vol. 46, No. 1, 72–81.

Gazis, D. C., 1959, "Three-dimensional Investigation of the Propagation of Waves in Hollow Circular Cylinders," *Journal of the Acoustical Society of America*, Vol. 31, No. 5, 568–578.

Giurgiutiu, V., 2003, "Lamb Wave Generation with Piezoelectric Wafer Active Sensors for Structural Health Monitoring," in *Proceedings of the SPIE 10th Annual International Symposium on Smart Structures and Materials and 8th Annual International Symposium on NDE for Health Monitoring and Diagnostics*, March 2–6, San Diego, CA, paper 5056-17.

Giurgiutiu, V. and Bao, J., 2002, "Embedded Ultrasonic Structural Radar for the Non-destructive Evaluation of Thin-wall Structures," in *Proceedings of the 2002 ASME International Mechanical Engineering Congress*, November 17–22, New Orleans, LA, paper IMECE2002-39017.

Giurgiutiu, V. and Zagrai, A., 2000, "Characterization of Piezoelectric Wafer Active Sensors," *Journal of Intelligent Material Systems and Structures*, Vol. 11, 959–976.

Giurgiutiu, V., Redmond, J., Roach, D., and Rackow, K., 2000, "Active Sensors for Health Monitoring of Aging Aerospace Structures," in *Conference on Smart Structures and Integrated Systems*, Newport Beach, CA, *Proceedings of the SPIE,* Vol. 3985, 294–305.

Giurgiutiu, V., Bao, J., and Zhao, W., 2003, "Piezoelectric Wafer Active Sensor Embedded Ultrasonics in Beams and Plates," *Experimental Mechanics*, Vol. 43, No. 4, 428–449.

Giurgiutiu, V., Yu, L., and Thomas, D., 2004, "Embedded Ultrasonic Structural Radar with Piezoelectric Wafer Active Sensors for Damage Detection in Cylindrical Shell Structures," in *Proceedings of the 45th AIAA/ASME/ASCE/AHS/ASC Structures, Structural Dynamics and Materials Conference and 12th AIAA/ASME/AHS Adaptive Structures Forum*, April 19–22, Palm Springs, CA, paper AIAA-2004-1983.

Goodman, L. E., 1952, "Circular-crested Vibrations of an Elastic Solid Bounded by Two Parallel Planes," in *Proceedings of the 1st National Congress of Applied Mechanics*, ASME, New York, 65–73.

Graff, K. F., 1975, *Wave Motion in Solids*, Dover, New York.

Ihn, J-B., 2003, "Built-in Diagnostics for Monitoring Fatigue Crack Growth in Aircraft Structures," Ph.D. Dissertation, Stanford University, Department of Aeronautics and Astronautics.

Ihn, J-B. and Chang, F-K., 2002, "Multicrack Growth Monitoring at Riveted Lap Joints Using Piezoelectric Patches," in *7th Annual International Symposium on Non-destructive Evaluation for Health Monitoring and Diagnostics*, March 17–21, San Diego, CA, *Proceedings of the SPIE,* Vol. 4702, 29–40.

Ing, R. K. and Fink, M., 1998, 'Time-reversed Lamb Waves," *IEEE Transactions on Ultrasonics, Ferroelectrics, and Frequency Control*, Vol. 45, No. 4, 1032–1043.

Janos, B. Z. and Hagood, N. W., 1998, "Overview of Active Fiber Composites Technologies," in *Proceedings of the 6th International Conference on New Actuators, ACTUATOR 98*, Bremen, Germany.

Keilers, C. H. and Chang, F-K., 1995, "Identifying Delaminations in Composite Beams Using Built-in Piezoelectrics: Part I – Experiments and Analysis; Part II – An Identification Method," *Journal of Intelligent Material Systems and Structures*, Vol. 6, 649–672.

Kessler, S. S., 2002, "Piezoelectric-based *In Situ* Damage Detection of Composite Materials for Structural Health Monitoring Systems," Ph.D. Dissertation, MIT, Cambridge, MA.

Koh, Y. L., Chiu, W. K., Rajic, N., and Galea, S. C., 2003, "Detection of Disbond Growth in a Cyclically Loaded Bonded Composite Repair Patch Using Surface-mounted Piezoceramic Elements," *Structural Health Monitoring – An International Journal*, Vol. 2, No. 4, 327–340.

Krautkramer, 1998, "Emerging Technology – Guided Wave Ultrasonics," *NDTnet*, Vol. 3, No. 6, http://www.ndt.net/article/0698/kk_gw/kk_gw.htm.

Krautkramer, 2002, *Products Catalog*, http://www.geinspectiontechnologies.com/solutions/TestingMachines/Ultrasonics/phasedarray.html

Krautkramer, J. and Krautkramer, H., 1990, *Ultrasonic Testing of Materials*, Springer-Verlag, Berlin.

Kudva, J. N., Marandis, C., and Gentry, J., 1993, "Smart Structures Concepts for Aircraft Structural Health Monitoring," *Proceedings of the SPIE*, Vol. 1917, 964–971.

Kwun, H. and Bartels, K. A., 1998, "Magnetostrictive Sensors Technology and its Applications," *Ultrasonics*, Vol. 36, 171–178.

Kwun, H., Light, G. M., Kim, S. Y., Peterson, R. H., and Spinks, R. L., 2002, "Permanently Installable, Active Guided Wave Sensor for Structural Health Monitoring," in *First European Workshop on Structural Health Monitoring* 2002, DEStech Pub, 390–397.

Lamb, H., 1917, "On Waves in an Elastic Plate," *Proceedings of the Royal Society of London*, *Series A,* Vol. 93, 114.

Lakshmanan, K. A. and Pines, D. J., 1997, "Modeling Damage in Composite Rotorcraft Flexbeams Using Wave Mechanics," *Smart Materials and Structures,* Vol. 6, No. 3, 383–392.

Lee, B. C. and Staszewski, W. J., 2003, "Modeling of Lamb Waves for Damage Detection in Metallic Structures: Part I – Wave Propagation; Part II – Wave Interactions With Damage," *Smart Materials and Structures*, Vol. 12, 804–814.

Lee, B. C., Palacz, M., Krawczuk, M., Ostachowicz, W., and Staszewski, W. J., 2004, "Wave Propagation in a Sensor/Actuator Diffusion Bond Model," *Journal of Sound and Vibration,* Vol. 276, No. 3–5, 671–687.

Lemistre, M., Gouyon, R., Kaczmarek, H., and Balageas, D., 1999, "Damage Localization in Composite Plates Using Wavelet Transform Processing on Lamb Wave Signals," in *Proceedings of the 2nd International Workshop of Structural Health Monitoring*, September 8–10, Stanford University, CA, 861–870.

Lemistre, M., Osmont, D., and Balageas, D., 2000, "Active Health System Based on Wavelet Transform Analysis of Diffracted Lamb Waves," *Proceedings of the SPIE*, Vol. 4073, 194–202.

Light, G. M., Kwun, H., Kim, S. Y., and Spinks, R. L., 2002, "Magnetostrictive Sensor Technology for Monitoring Bondline Quality and Defect Growth Under Adhesively Bonded Patches on Simulated Wing Structure," in *Proceedings of the 6th Joint FAA/DOD/NASA Conference on Aging Aircraft*, September 16–19, San Francisco, CA.

Lin, X. and Yuan, F. G., 2001a, "Diagnostic Lamb Waves in an Integrated Piezoelectric Sensor/Actuator Plate: Analytical and Experimental Studies," *Smart Materials and Structures*, Vol. 10, 907–913.

Lin, X. and Yuan, F. G., 2001b, "Damage Detection of a Plate using Migration Technique," *Journal of Intelligent Material Systems and Structures*, Vol. 12, No. 7, 469–482.

Lin, X. and Yuan, F. G., 2001c, "Detection of Multiple Damage by Prestack Reverse-time Migration," *AIAA Journal*, Vol. 39, No. 11, 2206–2215.

Lin, X. and Yuan, F. G., 2005, "Experimental Study of Applying Migration Technique in Structural Health Monitoring," *Structural Health Monitoring – An International Journal,* in press.

Liu, T., Veidt, M., and Kitipornchai, S., 2003, "Modeling the Input–output Behavior of Piezoelectric Structural Health Monitoring Systems for Composites Plates," *Smart Materials and Structures*, Vol. 12, 836–844.

Love, A. E. H., 1926, *Some Problems of Geodynamics*, Cambridge University Press, Cambridge.

Love, A. E. H., 1944, *A Treatise on the Mathematical Theory of Elasticity*, Dover, New York.

Lowe, M. J. S. and Cawley, P., 1994, "The Applicability of Plate Wave Techniques for the Inspection of Adhesive and Diffusion Bonded Joints," *Journal of Nondestructive Evaluation*, Vol. 13, 185–199.

Luo, W., Rose, J. L., and Kwun, H., 2003, "A Two-dimensional Model for Crack Sizing in Pipes," *Review of Progress in Quantitative Nondestructive Evaluation*, Vol. 23, 187–192.

Mal, A. K., Ricci, F., Gibson, S., and Banerjee, S., 2003, "Damage Detection in Structures from Vibration and Wave Propagation Method," *Proceedings of the SPIE*, Vol. 5047, 202–210.

Mason, G., 2002, "Identifying Damage Sensitive, Environmental Insensitive Features for Damage Detection," in *Proceedings of the 3rd International Conference on Identification in Engineering Systems*, University of Wales, Swansea, UK.

Moetakef, M. A., Joshi, S. P., and Lawrence, K. L., 1996, "Elastic Wave Generation by Piezoceramic Patches," *AIAA Journal*, Vol. 34, 2110–2117.

Monkhouse, R. S. C., Wilcox, P. D., and Cawley, P., 1996, "Flexible Interdigital PVDF Lamb Wave Transducers for the Development of Smart Structures," *Revue of Progress in Nondestructive Evaluation,* Vol. 16A, 877–884.

Monkhouse, R. S. C., Wilcox, P. D., Lowe, M. J. S., Dalton, R. P., and Cawley, P., 2000, "The Rapid Monitoring of Structures Using Interdigital Lamb Wave Transducers," *Smart Materials and Structures*, Vol. 9, 304–309.

Monier, T., Guy, P., Jayet, Y., Baboux, J. C., and Salvia, M., 2000, "Health Monitoring of Smart Composite Structures Using Ultrasonic Guided Waves," in 5*th European Conference on Smart Structures and Materials*, *Proceedings of the SPIE*, Vol. 4073, 173–181.

Moulin, E., Assaad, J., Delebarre, C., Kaczmarek, H., and Balageas, D., 1997, "Piezoelectric Transducers Embedded in a Composite Plate: Application to Lamb Wave Generation," *Journal of Applied Physics*, Vol. 82, No. 5, 2049–2055.

Moulin, E., Bourasseau, N., Assaad, J., and Delebarre, C., 2003, "Lamb Wave Beam Steering for Integrated Health Monitoring Applications," *Proceedings of the SPIE*, Vol. 5046, 124–131.

Osmont, D., Barnoncel, D., Devillers, D., and Dupont, M., 2002 "Health Monitoring of Sandwich Plates Based on the Analysis of the Interaction of Lamb Waves with Damages", in *Structural Health Monitoring 2002*, D. L. Balageas (Ed.), DEStech Pub, 2002, pp. 336–343.

Park, H. W., Sohn, H., Law, K. H., and Farrar, C. R., 2004, "Time Reversal Active Sensing for Health Monitoring of a Composite Plate," *Journal of Sound and Vibration,* in press, (available online at http://www.sciencedirect.com/science/journal/002246OX).

Pierce, S., Staszewski, W., Gachagan, A., James, I., Philip, W., Worden, K., Culshaw, B., McNab, A., Tomlinson, G., and Hayward, G., 1997, "Ultrasonic Condition Monitoring of Composite Structures Using a Low Profile Acoustic Source and an Embedded Optical Fiber Sensor," *Proceedings of the SPIE*, Vol. 3041, 437–448.

Pierce, S., Culshaw, B., Manson, G., Worden, K., and Staszewski, W., 2000, "The Application of Ultrasonic Lamb Wave Techniques to the Evaluation of Advanced Composite Structures," *Proceedings of the SPIE*, Vol. 3986, 93–103.

Purekar, A. and Pines, D. J., 2003, "Damage Interrogation Using a Phased Piezoelectric Sensor/Actuator Array: Simulation Results on Two-dimensional Isotropic Structures," in *Proceedings of the 44th AIAA/ASME/ASCE/AHS Structures, Structural Dynamics, and Materials Conference*, April 7–10, Norfolk, VA, paper AIAA 2003-1565, 1–9 (CD ROM).

Qing, X., Beard, S. J., and Kumar, A., 2003, "Optimal Placement of Sensor/Actuator in SMART Layer for Structural Health Monitoring," *Structural Health Monitoring – An International Journal,* in press.

Raghavan, A. and Cesnik, C. E. S., 2004, "Modeling of Piezoelectric-based Lamb Wave Generation and Sensing for Structural Health Monitoring," *Proceedings of the SPIE*, Vol. 5391, 419–430.

Rayleigh, J. W. S., 1887, "On Waves Propagated along the Plane Surface of an Elastic Solid," *Proceedings of the London Mathematical Society*, Vol. 17, 4–11.

Rizzo, P. and Lanza di Scalia, F., 2004, "Discrete Wavelet Transform to Improve Guided-wave-based Health Monitoring of Tendons and Cables," *Proceedings of the SPIE*, Vol. 5391, 523–532.

Rose, J. L., 1995, "Recent Advances in Guided Wave NDE," in *1995 IEEE Ultrasonics Symposium*, Cannes, France, 761–770.

Rose, J. L., 1999, *Ultrasonic Waves in Solid Media*, Cambridge University Press, Cambridge.

Rose, J. L., 2001, "A Vision of Ultrasonic Guided Wave Inspection Potential," in *Proceedings of the 7th ASME NDE Topical Conference,* NDE Vol. 20, 1–5.

Rose, J. L., Ditri, J. J., Pilarski, A., Rajana, K., and Carr, F. T., 1994, "A Guided Wave Inspection Technique for Nuclear Steam Generator Tubing," *NDT&E International*, Vol. 27, 307–310.

Rose, J. L., Rajana, K. M., and Hansch, K. T., 1995, "Ultrasonic Guided Waves for NDE of Adhesively Bonded Structures," *Journal of Adhesion*, Vol. 50, 71–82.

Rose, J. L., Rajana, K. M., and Barnisher, J. N., 1996, "Guided Waves for Composite Patch Repair of Aging Aircraft," in *Review of Progress in Quantitative Nondestructive Evaluation*, Plenum Press, New York, Vol. 15, 1291–1298.

Royer, D. and Dieulesaint, E., 2000, *Elastic Waves in Solids*, Springer-Verlag, Berlin.

Schwartz, W. G., Read, M. E., Kremer, M. J., Hinders, M. K., and Smith, B. T., 1999, "Lamb Wave Tomographic Imaging System for Aircraft Structural Health Assessment," in *Conference on Non-destructive Evaluation of Aging Aircraft, Airports, and Aerospace Hardware III*, Newport Beach, CA, *Proceedings of the SPIE,* Vol. 3586, 292–296.

Silk, M. G. and Bainton, K. F., 1979, "The Propagation in Metal Tubing of Ultrasonic Wave Modes Equivalent to Lamb Waves," *Ultrasonics*, January, 11–19.

Silvia, M. T., 1987, "Time Delay Estimation," in *Handbook of Digital Signal Processing*, D. F. Elliot, ed., Academic Press, New York.

Sohn, H., Wait, J. R., Park, G., and Farrar, C. R., 2004a, "Multiscale Structural Health Monitoring for Composite Structures," in *Proceedings of the 2nd European Workshop on Structural Health Monitoring*, July 7–9, Munich, Germany, 721–729.

Sohn, H., Park, G., Wait, J. R., Limback, N. P., and Farrar, C. R., 2004b, "Wavelet-based Active Sensing for Delamination Detection in Composite Structures," *Smart Materials and Structures*, Vol. 13, No. 1, 153–160.

Staszewski, W. J., Pierce, S. G., Worden, K., and Culshaw, B., 1999, "Cross-wavelet Analysis for Lamb Wave Damage Detection in Composite Materials using Optical Fiber," *Key Engineering Materials*, Vol. 167–168, 373–380.

Staszewski, W., Boller, C., and Tomlinson, G., 2004, *Health Monitoring of Aerospace Structures*, Wiley, New York.

Stoneley, R., 1924, "Elastic Waves at the Surface of Separation of Two Solids," *Proceedings of the Royal Society of London*, *Series A*, Vol. 106, 416–428.

Su, Z. and Ye, L., 2004, "Fundamental Lamb Mode-based Delamination Detection for CF/CP Composite Laminates Using Distributed Piezoelectrics," *Structural Health Monitoring – An International Journal*, Vol. 3, No. 1, 43–68.

Sundaraman, S. and Adams, D. E., 2002, "Phased Transducer Arrays for Structural Diagnostics Through Beamforming," in *Proceedings of the 17th Technical Conference of the American Society for Composites*, October 21–23, West Lafayette, IN, Paper 177.

Talbot, D., 2003, "Boeing's Flight for Survival," *Technology Reviews – MIT Magazine of Innovation*, September, 34–44.

Van Way, C. B., Kudva, J. N., Schoess, J. N., Zeigler, M. L., and Alper, J. M., 1995, "Aircraft Structural Health Monitoring System Development – Overview of the Air Force/Navy Smart Metallic Structures Program," *Proceedings of the SPIE*, Vol. 2443, 277–284.

Viktorov, I. A., 1967, *Rayleigh and Lamb Waves – Physical Theory and Applications*, Plenum Press, New York.

Wang, C. S. and Chang, F-K., 1999, "Built-in Diagnostics for Impact Damage Identification of Composite Structures," in *Structural Health Monitoring 2000*, Fu-Kuo Chang, ed., Technomic, Lancaster, PA, 612–621.

Wang, C. H., Rose, J. T., and Chang, F-K., 2003, "A Computerized Time-reversal Method for Structural Health Monitoring," *Proceedings of the SPIE*, Vol. 5046, 48–58.

Williams, R. B., Grimsley, B. W., Inman, D. J., and Wilkie, W. K., 2002, "Manufacturing and Mechanics-based Characterization of Macro Fiber Composite Actuators," *American Society of Mechanical Engineers, Aerospace Division, Publication AD* Vol. 67, 79–89.

Worlton, D. C., 1957, "Ultrasonic Testing with Lamb Waves," *Non-Destructive Testing*, Vol. 15, 218–222.

Worlton, D. C., 1961, "Experimental Confirmation of Lamb Waves at Megacycles Frequencies," *Journal of Applied Physics*, Vol. 32, 967–971.

Zemenek, J., 1972, "An Experimental and Theoretical Investigation of Elastic Wave Propagation in a Cylinder," *Journal of the Acoustical Society of America*, Vol. 51, No, 1 (Part 2), 265–283.